



HAL
open science

Arabidopsis seed mitochondria are bioenergetically active immediately upon imbibition and specialize via biogenesis in preparation for autotrophic growth

Gaël Paszkiewicz, Jose M. Gualberto, Abdelilah Benamar, David Macherel,
David Logan

► To cite this version:

Gaël Paszkiewicz, Jose M. Gualberto, Abdelilah Benamar, David Macherel, David Logan. Arabidopsis seed mitochondria are bioenergetically active immediately upon imbibition and specialize via biogenesis in preparation for autotrophic growth. *The Plant cell*, 2017, 29 (1), pp.109-128. 10.1105/tpc.16.00700 . hal-01605053

HAL Id: hal-01605053

<https://hal.science/hal-01605053>

Submitted on 26 May 2020

HAL is a multi-disciplinary open access archive for the deposit and dissemination of scientific research documents, whether they are published or not. The documents may come from teaching and research institutions in France or abroad, or from public or private research centers.

L'archive ouverte pluridisciplinaire **HAL**, est destinée au dépôt et à la diffusion de documents scientifiques de niveau recherche, publiés ou non, émanant des établissements d'enseignement et de recherche français ou étrangers, des laboratoires publics ou privés.

Copyright



Arabidopsis Seed Mitochondria Are Bioenergetically Active Immediately upon Imbibition and Specialize via Biogenesis in Preparation for Autotrophic Growth^{OPEN}

Gaël Paszkiewicz,^a José M. Gualberto,^b Abdelilah Benamar,^a David Macherel,^a and David C. Logan^{a,1}

^aIRHS, Université d'Angers, INRA, AGROCAMPUS-Ouest, SFR 4207 QUASAV, 49071 Beaucouzé cedex, France

^bInstitut de Biologie Moléculaire des Plantes, CNRS UPR2357, Université de Strasbourg, 67084 Strasbourg, France

ORCID IDs: 0000-0001-5060-9162 (G.P.); 0000-0002-7296-2618 (J.M.G.); 0000-0002-3352-2185 (D.M.); 0000-0002-8980-240X (D.C.L.)

Seed germination is a vital developmental transition for production of progeny by sexual reproduction in spermatophytes. Quiescent cells in nondormant dry embryos are reawakened first by imbibition and then by perception of germination triggers. Reanimated tissues enter into a germination program requiring energy for expansion growth. However, germination requires that embryonic tissues develop to support the more energy-demanding processes of cell division and organogenesis of the new seedling. Reactivation of mitochondria to supply the required energy is thus a key process underpinning germination and seedling survival. Using live imaging, we investigated reactivation of mitochondrial bioenergetics and dynamics using *Arabidopsis thaliana* as a model. Bioenergetic reactivation, visualized by presence of a membrane potential, is immediate upon rehydration. However, reactivation of mitochondrial dynamics only occurs after transfer to germination conditions. Reactivation of mitochondrial bioenergetics is followed by dramatic reorganization of the chondriome (all mitochondrial in a cell, collectively) involving massive fusion and membrane biogenesis to form a perinuclear tubuloreticular structure enabling mixing of previously discrete mitochondrial DNA nucleoids. The end of germination coincides with fragmentation of the chondriome, doubling of mitochondrial number, and heterogeneous redistribution of nucleoids among the mitochondria, generating a population of mitochondria tailored to seedling growth.

INTRODUCTION

Seed germination is a remarkable transition in the life cycle of spermatophytes, whereby the next generation sprouts from the dead protective tissues of the mother plant. The Greek philosopher Theophrastus (circa 372–287 BC) knew that food reserves were stored in seeds (Baskin and Baskin, 2014), but hundreds of years later, in the 17th century, many who wondered about the miraculous regeneration they witnessed considered germination to be essentially ex nihilo (Preston, 2009), since not only were dry seeds usually tiny compared with the size of the mature plant, but they lacked signs of life. Humankind, collectively fascinated by mortality, has long been fascinated with the reanimation that results in seed germination.

Seeds of the model plant *Arabidopsis thaliana* are composed of an embryo, charged with protein reserves, surrounded by two envelopes: the endosperm and the multilayered testa (Debeaujon et al., 2000). Following maturation and after-ripening to overcome dormancy, the seed is in a quiescent state, awaiting favorable conditions for germination (Finkelstein et al., 2008; Baskin and Baskin, 2014). Upon perception of the appropriate environmental conditions, germination of *Arabidopsis* proceeds in two sequential steps: The first step involves expansion of the

embryonic axis leading to rupture of the testa (Liu et al., 2005), while the second step involves elongation growth of the lower hypocotyl to drive protrusion of the radicle through the endosperm (Sliwinska et al., 2009). The reactivation of growth requires energy and, thus, reactivation of primary metabolism. However, mitochondria in dry seed are in a state of suspended animation and are structurally and functionally deficient relative to typical mitochondria extracted from mature tissue, lacking defined cristae and internal structure (Logan et al., 2001; Howell et al., 2006; Attucci et al., 1991). Thus, for many years, researchers have investigated the extent to which these rudimentary mitochondria, termed promitochondria, are functional early during imbibition and the processes, collectively termed biogenesis, that are responsible for their full reactivation (Logan et al., 2001; Howell et al., 2006; Dai et al., 1998; Ehrenshaft and Brambl, 1990). Many of the results from those studies were obtained from experiments performed in vitro, on cell-free homogenates derived from thousands of cells, originating from a mix of embryonic tissues; thus, interpretation is hampered by dilution and averaging errors. Nevertheless, those studies demonstrated that although mitochondria isolated from dry embryos had low tricarboxylic acid cycle enzyme activities, they were able to oxidize supplied succinate and/or NADH, enabling the generation of a membrane potential needed for protein import crucial for biogenesis (Ehrenshaft and Brambl, 1990; Logan et al., 2001; Howell et al., 2006; Benamar et al., 2003). However, because isolation procedures necessarily involved several hours of hydration, questions remained about the true state of promitochondria in vivo. In a recent study, primarily focused on changes in transcript abundance previously published by Narsai et al. (2011), Law et al. (2012) used a mitochondrial targeted GFP

¹ Address correspondence to david.logan@univ-angers.fr.

The author responsible for distribution of materials integral to the findings presented in this article in accordance with the policy described in the Instructions for Authors (www.plantcell.org) is: David C. Logan (david.logan@univ-angers.fr).

^{OPEN}Articles can be viewed without a subscription.

www.plantcell.org/cgi/doi/10.1105/tpc.16.00700

Arabidopsis line (Carrie et al., 2007) to visualize mitochondria in germinating Arabidopsis seeds. However, in that study, mitochondria expressing GFP were not detected in the dry seed embryos. Because fluorescent proteins driven by the same promoter but targeted to peroxisomes or plastids were detected, it was concluded that the lack of a mitochondrial GFP signal from dry embryos reflected low mitochondrial mass or protein content (Law et al., 2012). GFP was detected in mitochondria after 48 h of stratification (imbibition in the dark at 4°C), leading to the conclusion that Arabidopsis seed mitochondria required extensive biogenesis at the end of stratification, marked by a transient increase in abundance of a subset of mitochondrial transcripts and concomitant mitochondrial mass increase, in order to become metabolically active (Law et al., 2012). This conclusion contrasts with the maize (*Zea mays*) and rice (*Oryza sativa*) studies that concluded import competent promitochondria were active from the start of imbibition, fueled by external NADH (Logan et al., 2001; Howell et al., 2006; Benamar et al., 2003). Furthermore, changes in mitochondrial mass in maize and rice only occur late during germination, rather than before germination has been triggered, as suggested by the Arabidopsis study. We decided to revisit the role of promitochondria during germination, taking an *in vivo* bioimaging approach to investigate the reactivation of mitochondria bioenergetics, dynamics, and biogenesis during germination of Arabidopsis. Here, we show that mitochondria expressing mitochondrial-targeted GFP (mito-GFP; Logan and Leaver, 2000) are readily visible in the living dry seed and demonstrate that Arabidopsis promitochondria are bioenergetically active immediately upon hydration. Our results demonstrate the transient generation of a remarkable mitochondrial architecture at the end of germination, which we propose promotes nucleomitochondrial communication during a doubling of mitochondrial mass via biogenesis. The doubling of mitochondrial mass is concurrent with a redistribution of the mitochondrial genome to generate a functionally heterogeneous population of physically discrete but regularly interacting organelles. We hypothesize that this genetic discontinuous whole (Logan, 2006) is tailored to the changing role of mitochondria from the primary role of promitochondria as mitochondrial DNA (mtDNA)-containing molecular scaffolds to a mixed population of organelles providing for the more complex metabolic needs of autotrophic life.

RESULTS

Seed Embryo Mitochondria Are Metabolically Reactivated within Minutes of Hydration

Mitochondria in the dry seed embryonic cotyledons of Arabidopsis lines stably expressing mito-GFP, under the control of the CaMV 35S promoter, can be observed *in vivo* by confocal laser scanning microscopy (CLSM) of freshly dissected tissue mounted in the nonaqueous liquid perfluorodecalin (PFD; Figure 1). It was not technically possible to achieve clean dissection of the intact whole embryo from the dry seed to enable *in vivo* imaging of tissue other than the cotyledon (due to their position close to the hilum scar), but 10 min of hydration

enabled complete embryo removal prior to mounting in PFD. This method demonstrated the even distribution of mito-GFP expressing mitochondria throughout the embryo (Figure 1A; Supplemental Movie 1) often arranged in what appeared to be small groups of two or three, but resolving these as independent objects was not possible within the limits of the imaging technology available. Next, we investigated whether or not mitochondria were bioenergetically active using the fluorescent lipophilic cationic dye tetra methyl rhodamine methyl ester (TMRM), which accumulates in mitochondria in inverse proportion to the membrane potential according to the Nernst equation (Brand and Nicholls, 2011). TMRM-stained structures were readily observed throughout the embryo within 15 min of imbibition (Figure 1B), and these structures colocalized (Mander's coefficient = 0.94 ± 0.05 , $n = 9$) with mito-GFP, confirming them as mitochondria.

Measurement of oxygen uptake (Figure 1C) demonstrated a rapid resumption of respiration upon rehydration of the dry seed at 21°C, with a progressive increase of O₂ consumption during the first hour of imbibition until full rehydration, as described before (Sew et al., 2013). Oxygen consumption was also monitored during imbibition and incubation of seeds for 48 h in the dark at 4°C, conditions that correspond to the stratification treatment widely used with Arabidopsis. Even after 3 h of imbibition in the dark, a significant level of O₂ consumption at 4°C was detected, revealing that resumption of mitochondrial respiration was also proceeding, albeit more slowly, at low temperature (Figure 1C). After 48 h at 4°C in the dark, oxygen consumption measured at 4°C had almost doubled but was still lower than if measured after imbibition at 21°C. Transfer of stratified seeds to 21°C in the light resulted in a >5-fold increase in oxygen consumption (Figure 1C), reflecting the thermal dependence of respiration and the high respiratory activity of the stratified seeds. From these data the Q₁₀ of respiration can be estimated between 2.46 and 3.22 [using the equation $Q_{10} = (R_2/R_1)^{(10/T_2-T_1)}$]. These relatively high values suggest that respiration of stratified seeds was not limited by substrate availability (Atkin and Tjoelker, 2003). Cyanide inhibited O₂ consumption more strongly at 21° than at 4°C, suggesting a higher capacity of the alternative pathway at low temperature, which agrees with the cold induction of alternative oxidase gene expression (Wang et al., 2011).

Together, these data show that mitochondria quickly regain membrane potential and metabolic activity upon embryo imbibition and that incubation at low temperature during stratification maintains a lower rate of metabolism because of the thermal constraint.

Mitochondrial Motility Increases in Response to Environmental Germination Cues

Given that Arabidopsis seed mitochondria regain bioenergetic activity within 15 min of rehydration (Figure 1), we were interested to determine when during germination mitochondria regain motility. Mitochondria were immobile in the dry embryonic cotyledon (Supplemental Movie 1); however, challenging imaging conditions (slight tissue movement and general image clarity) prevented accurate quantification. After 12 h of stratification (Figure 2), mitochondria exhibited disordered localized oscillatory movements,

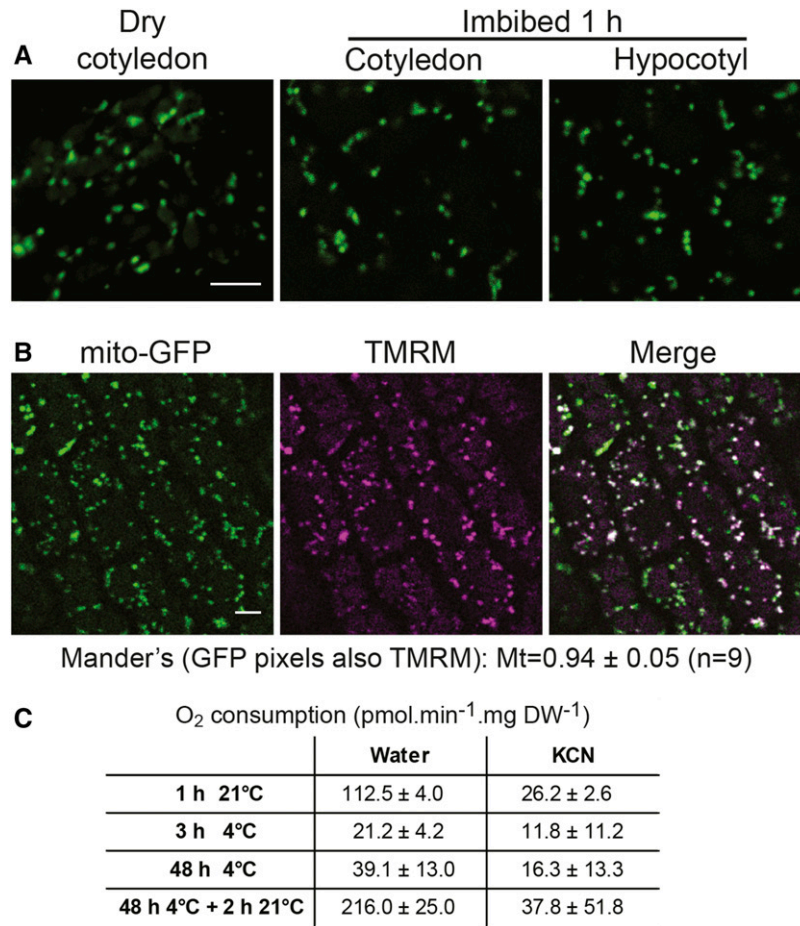


Figure 1. Mitochondria Are Clearly Detectable in the Dry Embryo and Are Bioenergetically Reactivated within Minutes of Hydration.

(A) Images of embryo mitochondria from seed expressing mito-GFP under control of 35S promoter. Seed were either dry or imbibed at 4°C in the dark. Embryos were mounted in PFD to avoid tissue hydration and observed within 5 min. Bar = 5 μm .

(B) Colocalization of TMRM, a reporter of membrane potential, and mito-GFP in cotyledon mitochondria. The majority of mitochondria in the merged image display white pixels indicating colocalization of TMRM (magenta) and GFP (green). Quantification of colocalization is provided by the Mander's coefficient below images ($\pm\text{SE}$, $n = 9$). Bars = 5 μm .

(C) Measurement of respiration in mito-GFP seed after the first hours of imbibition, at the end of stratification, and upon transfer to germination promoting conditions. Cyanide (500 μM KCN) was used to estimate alternative pathway capacity.

generating low displacement values and track straightness (Figures 2D and 2E; Supplemental Movie 1), with three-quarters of mitochondria displaying speeds <6.1 nm/s (Figure 2C; Supplemental Movie 1). This pattern of mitochondria motility was maintained until the seeds were transferred, after 48 h of imbibition, to the illuminated growth chamber at 21°C (Figures 2C to 2E; Supplemental Movie 1). After 50 h of imbibition, i.e., 2 h after transfer to germination-promoting conditions, 75% of mitochondria displayed increased speeds (>5.9 nm/s) and directional movements, as indicated by a clear shift to larger track straightness values over increased track displacement distances (Figures 2B to 2E; Supplemental Movie 1). The increased motility of physically discrete mitochondria increased the number of encounters between them and the fusion rate (measured with the Imaris software, as the rate that two surface objects connect), leading to a higher percentage of interacting mitochondria in the

population (Figures 2F to 2H). As germination progressed, mitochondrial movement continued to be more organized up to the stage of testa rupture (TR): Mitochondria moved at higher speeds and generated longer, straighter tracks. This increase in mitochondrial motility was accompanied by a peak in the percentage of mitochondria interacting (Figure 2F), the number of mitochondria in each interaction node (defined by sharing a track; Figure 2G), and the number of fusion events per mitochondrion (note the relatively large spread between the first and third quartiles; Figure 2H), as distantly located mitochondria met and underwent interaction. At the end of germination (endosperm rupture [ER] stage), there was a reduction in the values of mitochondrial dynamics parameters, marking the end of the transient burst of activity facilitating mitochondrial interaction and fusion. The reduction in mitochondrial speed, displacement and track straightness was concurrent with a reduction in the percentage of

mitochondria interacting, the number of mitochondria in each interaction node, and a reduction in the number of fusion events per mitochondrion (Figure 2).

Mitochondrial motility increased once more at the root hair (RH) stage, coincident with greening of the cotyledons, leading to increased interaction and transient fusion between mitochondria. Because our methods were tailored to the low speeds of mitochondria movement in germinating seeds, relative to the speeds in leaves of young seedlings (Supplemental Figure 1), the values recorded at the RH stage are underestimated, since high velocity mitochondria entered and left the focal plane faster than the image capture rate. For example, mitochondria in green cotyledons of 4-d-old seedlings move with an average speed of 140 nm s^{-1} , with a peak of 363 nm s^{-1} relative to an average of 14 nm s^{-1} at the RH stage (compared with Figure 2B and Supplemental Figure 1B).

Our experimental procedure included 48 h of stratification (4°C , dark) in order to ensure synchronous germination and consistency in the physiological stage of embryos selected at fixed time points. This is the method of choice at early stages of development, when physical descriptors cannot be used, and allows comparison of our results with the two key transcriptomic studies of Narsai et al. (2011) and Law et al. (2012). However, we also investigated the reactivation of mitochondrial dynamics during germination in the absence of stratification to determine to what extent the key events observed are influenced by stratification per se (Supplemental Figure 2 and Supplemental Movie 2). Those results demonstrate that the reactivation of mitochondrial dynamics occurs similarly in stratified and non-stratified seeds, albeit faster with stratification (Supplemental Results and Supplemental Figure 2).

Mitochondrial Immobility during Early Germination Is Not Due to Defective Actin Dynamics

To further investigate the mechanism responsible for the almost complete absence of mitochondrial motility during imbibition, we first examined biogenesis of the F-actin cytoskeleton, which facilitates mitochondrial motility in Arabidopsis. Using a stable double-transgenic line expressing mito-GFP and the F-actin binding protein reporter mCherry-mTalin (ElZawily et al., 2014), we were able to observe a filamentous and dynamic F-actin cytoskeleton after 24 h of imbibition at 4°C , even though the mitochondria remained relatively immobile (Figure 3; Supplemental Movie 3). The F-actin cytoskeleton was more clearly defined against the background fluorescence at later stages of stratification and during germination, exhibiting a similarly dynamic filamentous network at the TR stage as observed at 24 h (Figure 3A; Supplemental Movie 3). Simultaneous observation of mitochondria and F-actin showed the mitochondria to be in close proximity to actin bundles and that remodeling of the F-actin was coincident with the small-scale localized changes in mitochondrial motion and morphology measured; mitochondria were not observed to track along F-actin during stratification (Figure 3B; Supplemental Movie 3).

Next, to test whether the lack of mitochondrial movement was specific, or due to a deficiency during early germination shared with other organelles, we investigated motility of the endoplasmic reticulum and of peroxisomes, organelles that also move on actin (Jedd and Chua, 2002; Ueda et al., 2010), using stable transgenic

lines expressing fluorescent proteins targeted to each organelle. The ER was observed as a network of tubular membranes at 24 h of stratification and toward the end of germination at the TR stage (Figure 3C). Quantification of ER dynamics by colocalization analysis demonstrated no difference between these two time points: Pearson coefficients of 0.67 ± 0.07 and 0.66 ± 0.06 ($n = 9$) at 24 h and TR stage, respectively (Figure 3C). In contrast, but similar to mitochondria, peroxisomes were relatively immobile after 24 h of imbibition in the dark at 4°C (Figure 3D). At that stage, peroxisomes exhibited localized erratic movements as observed for mitochondria. However, by the TR stage, when the chondriome (all mitochondrial in a cell, collectively) existed as perinuclear tubuloreticular structure driven by fusion between interacting mitochondria, peroxisome morphology and dynamics had changed relatively little and they only displayed an approximate doubling of speed of movement (from 3.58 to 6.7 nm/s) (Figure 3D).

Reactivation of Mitochondrial Dynamics during Germination Is Inhibited by Cold or Abscisic Acid and Promoted by the Gibberellic Acid Pathway

To understand what triggers the switch from relatively immobile to mobile mitochondria upon transfer of seeds to germination promoting conditions, we tested the effects on mitochondrial dynamics of various temperature, light, or hormone treatments. Transfer of stratified seed from 4 to 21°C leads to an increase in mitochondrial dynamics (Figure 4) both in the light (Figure 4A) and the dark (Figure 4B), although the movement in the light occurred at higher speeds and straighter trajectories, so generating longer displacement distances (Figures 4C to 4E). Mitochondria in seeds maintained at 4°C and transferred to light for 2 h (Figure 4, red outline) continued to display the same pattern of dynamics measured during stratification and shown in Figure 2B (48 h S).

Treatment with GA_3 in the light or dark had little effect on mitochondrial dynamics relative to the controls, beyond a shift in track straightness for the majority of the mitochondrial population (Figure 4). Treatment with abscisic acid (ABA; which inhibited germination; seeds did not develop beyond the TR stage) strongly reduced the activation of mitochondrial dynamics upon transfer of seed from stratification conditions to $21^\circ\text{C}/\text{light}$, such that measured parameters tended toward those measured for seeds maintained at 4°C (Figure 4). The larger interquartile range (IQR) for mitochondrial speeds suggests that ABA interfered with the homogenizing effect that transfer to light had on mitochondrial dynamics (Figure 4C). In contrast to the inhibitory effect of ABA treatment in the light, treatment with ABA in the dark had no observable effect on the measured mitochondrial dynamics parameters apart from an increase in track straightness (Figure 4). Paclobutrazol (which inhibited germination, no testa rupture) reduced mitochondrial speed and displacement in the light at 21°C relative to the control (Figures 4C and 4D), although less effectively than ABA. Similarly, paclobutrazol caused a reduction in the percentage of mitochondria interacting relative to those in untreated seed (Figure 4H). The inhibitory effects of paclobutrazol were only apparent in the light; seed treated with paclobutrazol but maintained in the dark displayed similar dynamics to untreated seed in the dark. ABA, and to a lesser extent, paclobutrazol, thus inhibited the activation of mitochondrial dynamics and interaction

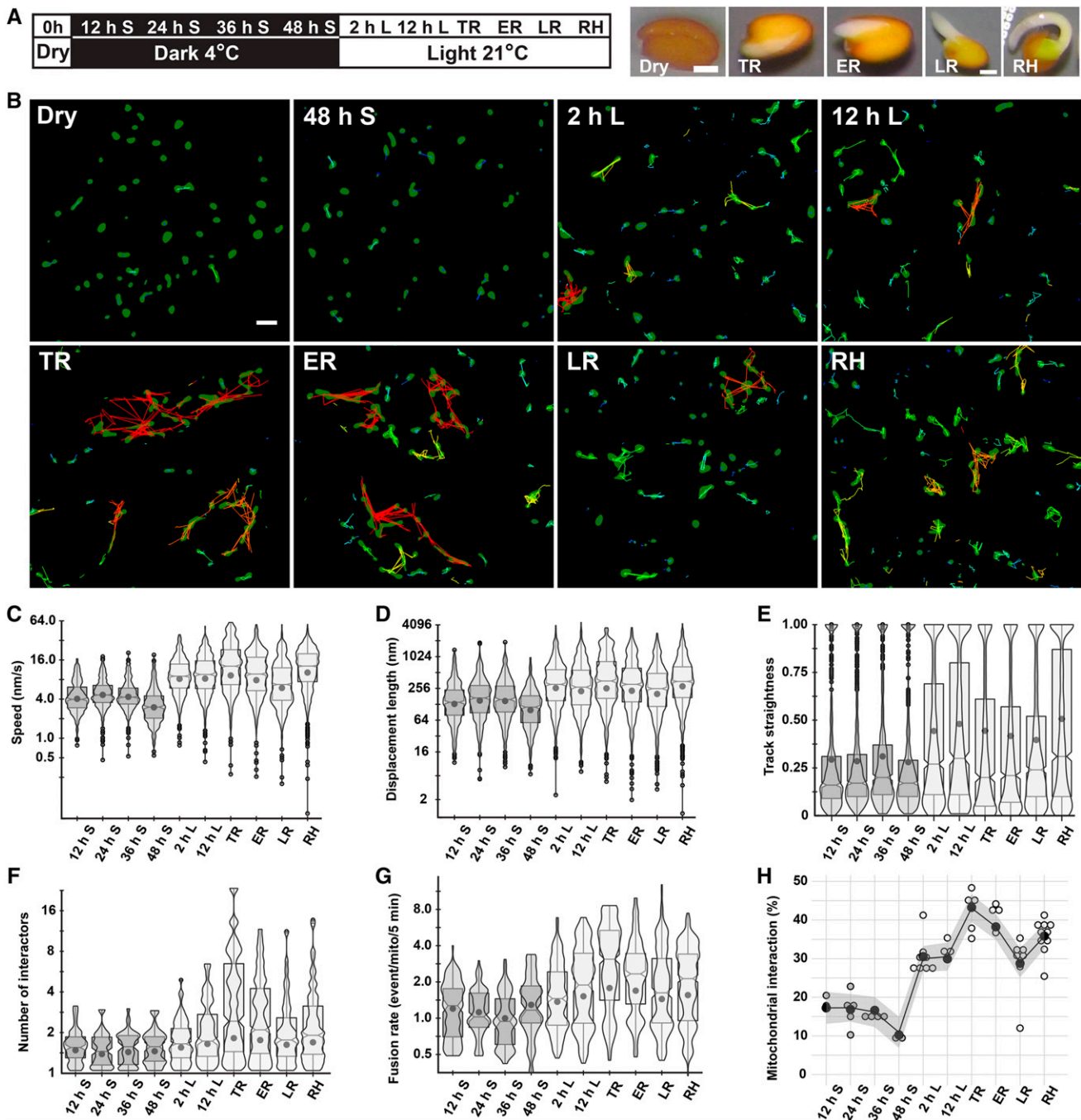


Figure 2. Mitochondrial Motility Increases in Response to Germination Cues and Leads to Increased Intermitochondrial Interaction and Fusion.

(A) Germination protocol and images of seed at the developmental stages used for experiments. Developmental stages: TR, testa rupture; ER, endosperm rupture; LR, long root; RH, root hair. L, after transfer to light; S, stratification. Bar = 200 μ m.

(B) Images generated using Imaris to track mitochondria in cotyledon cells over a period of 5 min. Detected mitochondria were colored green and tracks are rainbow colored according to speed (no movement is purple, and movement above 0.032μ m/s is red). Each image is representative of data captured from six seeds (total number of tracks analyzed per time point ranges from 623 to 2180). Bar = 5 μ m. See Supplemental Movie 1.

(C) Violin box plots of the mean speed recorded per track in nanometers/second. Box plot whiskers indicate $1.5 \times$ IQR, and any outliers are represented by an open circle, as described by Tukey. Means are represented by a solid circle. The notch corresponds to the median $\pm 1.58 \times$ IQR/ \sqrt{n} .

(D) Violin box plots of track displacement length. Plot design as in **(C)**.

(E) Violin box plots of track straightness (1 = perfectly straight). Plot design as in **(C)**.

(F) Violin box plots of numbers of interactors per track for tracks having at least one interaction between detected mitochondrial objects. Plot design as in **(C)**.

in response to light. The effect of these drugs on mitochondrial dynamics therefore partly mirrors their effect on germination. Under germination-promoting conditions, mitochondrial dynamics are activated by gibberellic acid (GA) and inhibited by ABA or paclobutrazol.

Transfer of Seed to Germination-Promoting Conditions Induces Formation of ATG8-Labeled Autophagosomes

The promitochondria reactivated during imbibition have survived challenging conditions during seed drying, the dry state itself, and then strains imposed by rehydration. We therefore tested for the induction of autophagy following the initiation of imbibition and transfer to germination promoting conditions. To visualize and quantify the autophagy-related 8 (ATG8) protein labeled phagophores/autophagosomes (hereafter referred collectively as autophagosomes), we used lines expressing both mRFP1-ATG8F (Honig et al., 2012) and mito-GFP (Logan and Leaver, 2000). Automatic segmentation of the mRFP1 signal from autophagosomes was complicated due to the red autofluorescence of the protein storage vacuoles (PSVs). However, mRFP1-ATG8F could be detected by its brighter fluorescence, association into spheroid bodies of ~ 0.5 to $1 \mu\text{m}$ in diameter, and absence of characteristic PSV fluorescence at 425 to 475 nm upon excitation at 405 nm (Figure 5; Supplemental Movies 4 and 5). Due to the interfering autofluorescence, we were not able to automatically quantify colocalization with confidence; therefore, manual counts were made of the combined number of instances of close juxtaposition of mitochondria and mRFP1-ATG8F structures (Supplemental Movie 4; Figure 5) and instances where mitochondria appear enclosed by mRFP1-ATG8F (Supplemental Movie 5; Figure 5). Autophagosome number was very low after 48 h of stratification, with only 0.08 bodies visible per cotyledon epidermal pavement cell (Figure 5C). However, 6 h after transfer to germinating conditions (6 h L), a large increase in autophagosome number per cell was detected (Figure 5C). Concomitant with the increased autophagosome number, we observed that the majority of these bodies were closely associated with or colocalized with mitochondria (Figures 5B and 5C), suggesting their specific participation in mitophagy.

Activation of Mitochondrial Motility during Germination Leads to the Formation of a Tubuloreticular Chondriome through a Shift in the Fusion/Fission Balance

Mitochondrial motility is required to effect changes to mitochondrial number per cell and individual mitochondrial volume via the motility dependent processes of mitochondrial fusion and division. Thus, we next quantified these parameters to better understand mitochondrial dynamics during germination (Figure 6). Mitochondrial number decreased slightly during stratification

concomitant with a reduction in total mitochondrial volume (Figures 6A to 6C). The spherical morphology of mitochondria in dry seeds (Figure 1) was maintained during stratification, with more than 75% of the population having an object sphericity (OS) >0.8 (Figures 6A and 6D). Despite the relatively homogeneous morphology of mitochondria during stratification, the volume of individually resolvable mitochondria (mito-GFP objects) varied 1000-fold from 0.004 to $3.470 \mu\text{m}^3$ (Figure 6E).

Twelve hours after transfer to light/ 21°C (60 h from the start of imbibition), the number of mitochondria was unchanged, but they were more elongate (42% of mitochondria had a sphericity of <0.8 , median = 0.83) and individual mitochondria were larger (25% of objects had a volume greater than $0.43 \mu\text{m}^3$; Figure 6E). The changes of mitochondrial morphology observed at 60 h, from spherical to more elongate structures, continued over the next hours until the TR stage (Figure 6; Supplemental Movie 4). At the TR stage, most mitochondria displayed a tubular morphology with frequent branching (75% of objects had OS <0.9 ; Figures 6A and 6D; Supplemental Movie 6), thereby forming a tubuloreticular structure, with only $\sim 25\%$ of the population displaying sphericity values in the range previously observed for 75% of mitochondria during stratification (when 75% of mitochondria had a OS of >0.8 ; Figure 6D). The change in mitochondrial shape was accompanied by a shift in the volumes of individual organelles to larger values (over 25% of organelles had a volume between 0.54 and $38.7 \mu\text{m}^3$) and an increase in total chondriome volume (Figures 6C and 6E). The wide distribution of volumes also reflects the continued presence of small spherical mitochondria (similar as observed during stratification) that do not interact and remain as singletons. By the end of germination, ER stage, the number of reticular/tubular mitochondria had decreased with OS values rising (50% of objects had OS >0.8 and 50%). Mitochondria remained visibly clustered (Figure 6A, ER; Supplemental Movie 6), but the volumes of the largest objects were reduced, which together with the increased sphericity, reflects the change from a tubuloreticular chondriome to a more discontinuous population. The disassembly of the chondriome structure led to an increase in number of identifiable discrete mitochondria (Figures 6A and 6B). The disintegration of the mitochondrial reticulum and reduction in mitochondrial tubulation continued during early seedling growth such that by the long root (LR) stage over 75% of mitochondria had an OS >0.8 , and 50% had an OS >0.9 . This change in morphology was accompanied by a further reduction in the volumes of the largest objects (Figure 6E; Supplemental Movie 4) and associated reduction in morphological heterogeneity. In addition, the number of identifiable discrete mitochondria, which was observed to increase from the TR to the ER stage continued to rise through the LR and RH stages. By the time the seedling had developed root hairs (RH stage), mitochondria were typically round to ovoid, although some tubules were observed. The distribution of OS and

Figure 2. (continued).

(G) Violin box plots of the rate of fusion between mitochondrial objects expressed per mitochondria. Plot design as in **(C)**.

(H) Dot plot of the percentage of mitochondria sharing a track within the 5-min tracking period. Open circles indicate percentage mitochondrial objects sharing a track in each image stack, while the solid circle indicates the mean ($n = 6$). The line represents the Loess regression, while the gray area corresponds to the 95% confidence interval.

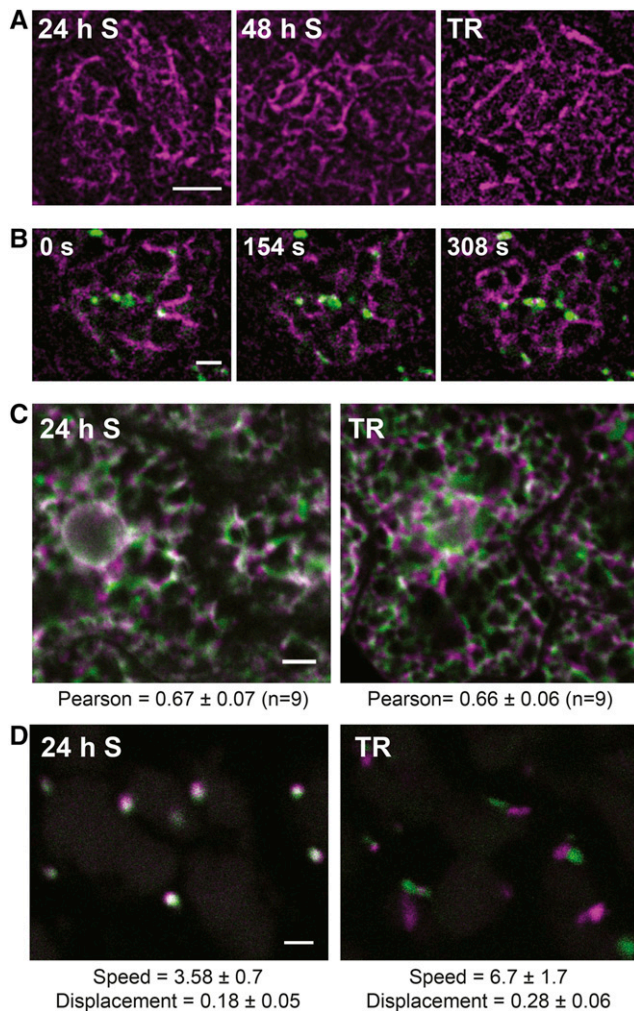


Figure 3. Measurement of Dynamic Reactivation of F-Actin, the Endoplasmic Reticulum, or Peroxisomes.

(A) Visualization of F-actin in cotyledon cells of a double transgenic line expressing mCherry-mTalin and mito-GFP during stratification, and near the end of germination. Bar = 5 μ m.

(B) Time-lapse series of images showing changes in position of mitochondria (green) as a result of limited reorganization of F-actin (magenta) that occurs during stratification (Supplemental Movie 3). Bar = 2 μ m.

(C) Images generated from the merging of two single frame optical slices, captured 5 min apart, of embryonic cotyledon cells expressing the endoplasmic reticulum marker YFP-HDEL after 24 h of imbibition in dark at 4°C or at the TR stage. The first image ($t = 0$) was false-colored green, the second ($t = 5$ min), magenta. White pixels indicate colocalization and, therefore, relative immobility. Pearson's colocalization coefficient is the average from the analysis of nine seeds. Bar = 5 μ m.

(D) Embryonic cotyledon cells expressing the peroxisomal marker YFP-SKL; images were captured as in **(C)**. Dynamics were measured by object tracking: speed is in nm/s and displacement in μ m. Measurement was performed on at least seven plants at each time point. Bar = 2 μ m.

individual organelle volume values were similar to those measured after 12 h 21°C/light, although mitochondria were more heterogeneous at the RH stage, particularly due to an increase in number of small mitochondria (Figures 6D and 6E). The increase in proportion of small mitochondria was concomitant with an increase in total mitochondrial number; consequently, there was little change in total mitochondrial volume (Figures 6C and 6E; Supplemental Movie 6).

The Mitochondrial Tubuloreticulum Formed during Late Germination Encircles the Nucleus

Our analysis of the 4D structure of the chondriome during germination showed an activation of mitochondrial dynamics that led to the generation of a tubuloreticular structure composed of tubular and/or branched mitochondria at the end of germination (TR/ER stages). To further investigate the subcellular location of this structure, we examined its localization with respect to PSVs, taking advantage of their specific autofluorescence (Bolte et al., 2011; Hunter et al., 2007; Fujii et al., 2007). In the dry seed, the PSVs were spherical to ovoid structures and filled much of the cell volume (Figure 7; as previously described by Bolte et al. [2011]). The spherical mitochondria were distributed seemingly randomly in the remaining cortical space and between the PSVs. Following transfer to light, the mitochondria congregated in the space between the PSVs (Figure 7A) and from 12 h of light (60 h time point) the congregated mitochondria formed the tubuloreticular structure in the PSV-free areas (Figure 7A). Following germination, when the tubular network disassembled, most mitochondria were redistributed more evenly within the cell (Figure 7A; see also Figures 2 and 6).

Our investigations on the nature of the organelle surrounded by the tubular mitochondria coincided with investigations of the abundance and distribution of mtDNA in vivo, using the DNA binding fluorescent dye SYBR Green I (see below), which also stains the nucleus (although not uniformly across cells) under longer staining times. We were therefore able to observe both mitochondria and the nucleus simultaneously, which revealed that, at the TR stage, when mitochondrial reticulation is most pronounced, SYBR Green I stained mtDNA nucleoids encircled the nucleus within a PSV-free area (Figure 7B; see also Figure 8A, panel TR).

The Perinuclear Mitochondria Enable Interaction and Redistribution of mtDNA Nucleoids at the End of Germination

The mtDNA is packaged into compact nucleoid structures composed of variable amounts of DNA and protein. Nucleoids are distributed heterogeneously within the mitochondrial population in tobacco (*Nicotiana tabacum*) and onion (*Allium cepa*) cells (Arimura et al., 2004; Sheahan et al., 2005) and can be redistributed by mitochondrial fusion and fission (Sheahan et al., 2005). We checked how remodeling of the chondriome during germination affected the distribution of mitochondrial nucleoids. By staining with SYBR Green I in a line expressing mCherry in the mitochondrial matrix (Candat et al., 2014), we were able to both visualize mtDNA and mitochondria in the embryo, from 10 min

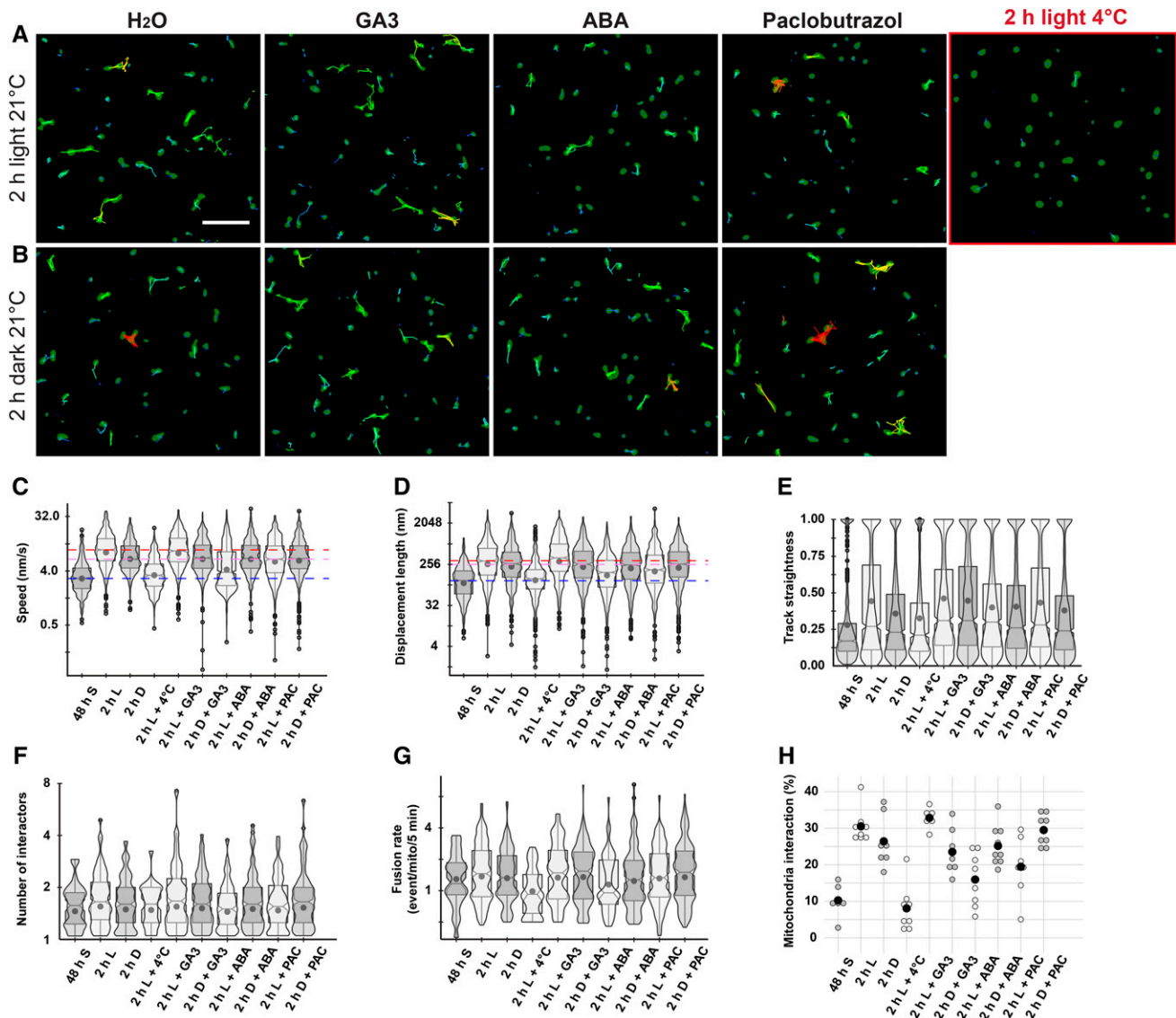


Figure 4. Effects of ABA, GA₃, and Paclobutrazol on the Reactivation of Mitochondrial Dynamics.

(A) Images generated using Imaris to track mitochondria in cotyledon cells, maintained throughout the time course in 100 μ M ABA, GA₃, or paclobutrazol, after stratification for 48 h at 4°C and 2 h after transfer to light/21°C. Detected mitochondria were colored green, and tracks are rainbow colored according to speed (no movement is purple, and movement above 0.032 μ m/s is red). Bar = 5 μ m.

(B) As in **(A)** but seeds were transferred to dark/21°C after 48 h of stratification. Bar = 5 μ m.

(C) Violin box plots of the mean speed recorded per track in nanometers/second. Box plot whiskers indicate 1.5 \times IQR, and any outliers are represented by an empty circle, as described by Tukey. Means are represented by a full circle. The notch corresponds to the median \pm 1.58 \times IQR/ \sqrt{n} . The colored lines indicate the median of the mean speed of mitochondria following 48 h of stratification (blue), 2 h after transfer to 21°C/dark (violet), or 21°C/light (red). Total number of objects tracked per time point ranges from 636 to 1386 from between six and nine seeds.

(D) Violin box plots of track displacement length. The blue, violet, and red lines indicate the median of the displacement length after 48 h of stratification (blue), 2 h after transfer to 21°C/dark (violet), or 21°C/light (red). Plot design as in **(C)**.

(E) Violin box plots of track straightness (1 = perfectly straight). Plot design as in **(C)**.

(F) Violin box plots of numbers of interactors per track for tracks having at least one interaction between detected mitochondrial objects. Plot design as in **(C)**.

(G) Violin box plots of the rate of fusion between mitochondrial objects expressed per mitochondria. Plot design as in **(C)**.

(H) Dot plot of the percentage of mitochondria sharing a track within the 5-min tracking period. Empty circles indicate percentage mitochondrial objects sharing a track in each image stack, while the full circle indicates the mean.

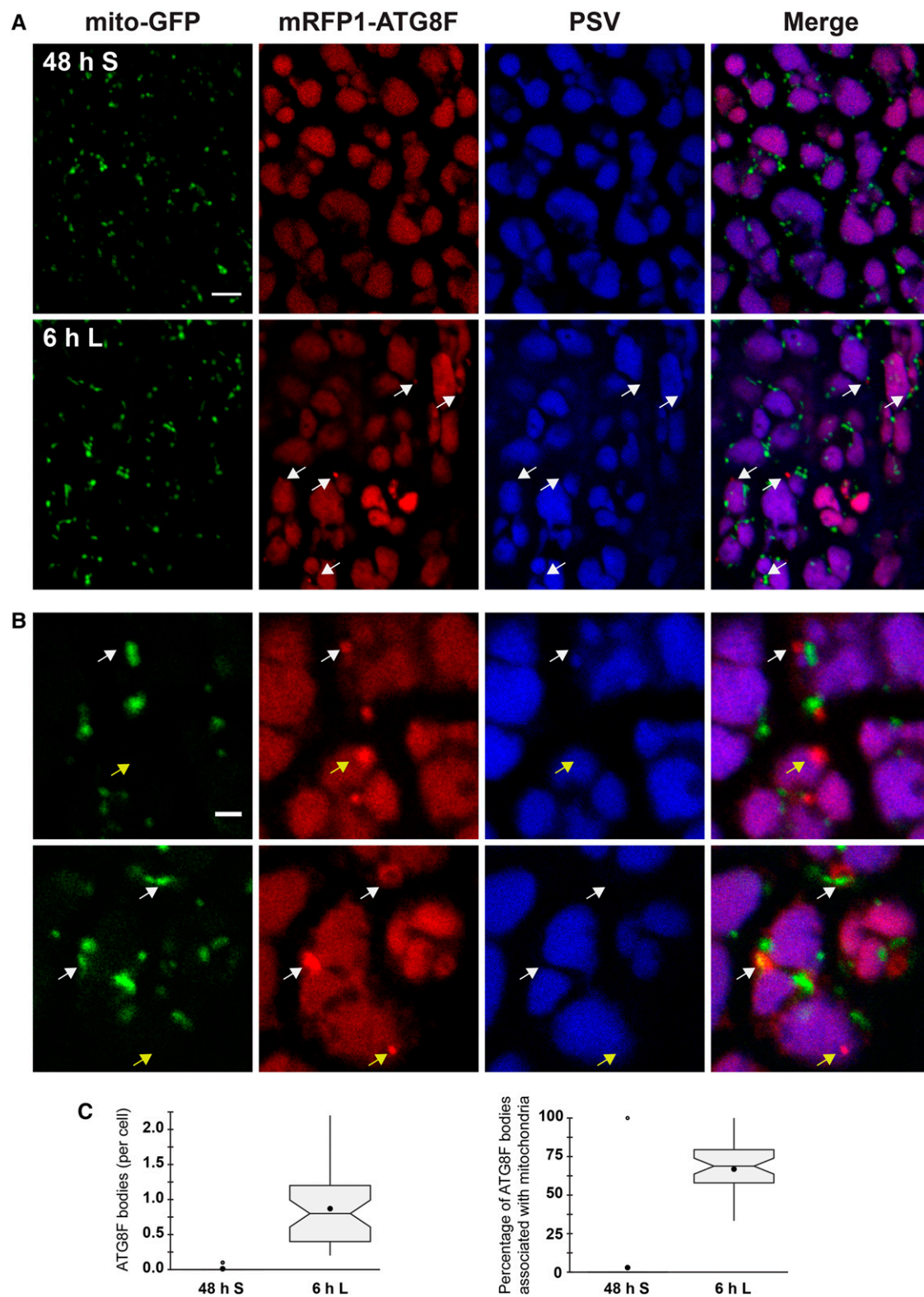


Figure 5. Transfer of Seed to Germination-Promoting Conditions Induces the Formation of ATG8F-Decorated Autophagosomes.

(A) Seed expressing both mito-GFP (green) and mRFP1-ATG8F (red) were observed by CLSM. PSV autofluorescence is colored blue. Bar = 5 μ m.

(B) Enlarged micrographs to show putative mitophagy during early germination. Arrows indicate ATG8F bodies, either associated with or surrounding mitochondria (white) or non-associated (yellow). Bars = 2 μ m. See also Supplemental Movies 4 and 5.

(C) Quantification of the numbers of ATG8F decorated bodies per cell and the percentage of ATG8F bodies close or containing mito-GFP signal. Data from 19 different embryos per time point from three independent experiments. Box plot whiskers indicate $1.5 \times$ IQR, and outliers are represented by an empty circle, as described by Tukey. Means are represented by a full circle. The notch corresponds to the median $\pm 1.58 \times$ IQR/ \sqrt{n} .

imbibition till the end of germination. Ninety-one percent of mitochondria contained detectable mtDNA at the onset of imbibition and during stratification (Figure 8). Quantitative fluorescence imaging revealed that there was little change in the average nucleoid fluorescence intensity (approximate measure of mtDNA content) or in the variation in fluorescence intensity within the nucleoids (measure of nucleoid compaction) during germination (Figures 8C and 8D). There was little change in the number of detectable mitochondrial nucleoids between the 48 h and TR stages (153 nucleoids per field compared with 163), but at TR, the percentage of mitochondria with detectable mtDNA dropped to 74% (Figure 8B). Since there was little change in the number of detectable mitochondria at 48 h compared with TR (168 per field versus 161; Figure 6B), this reduction in the percentage of mitochondria containing mtDNA was concomitant with an increase in the number of nucleoids per DNA-containing mitochondrion (Figure 8B). At the RH stage, fragmentation of the reticular mitochondria resulted in a 3-fold increase in the number of mitochondria per field of view (from 161 at TR to 480 per field at RH; Figure 6B). However, the number of detectable nucleoids only increased by ~2-fold (from an average of 163 per view at TR to 322 at the RH stage), such that redistribution of the nucleoids within the new fragmented structure resulted in further heterogeneity in the chondriome as the percentage of mitochondria containing detectable mtDNA dropped further to 67% (Figure 8B).

During stratification, there was no measurable movement of nucleoids within the mitochondria beyond the slight wobbling of mitochondria detected previously (Supplemental Movie 1). However, it was clear from time-lapse imaging that the redistribution of nucleoids within the chondriome during late germination was an active process combining mitochondrial movement and movement of the nucleoid within mitochondria, enabling transient association between mtDNA molecules that were previously segregated (Supplemental Movie 7).

mtDNA Quantity, Quality, and Recombination Are Tightly Controlled during Germination

Lack of mitochondrial motility inhibits mitochondrial fusion and therefore isolates the mtDNA within each physically discrete mitochondrion. We hypothesized that the lack of mitochondrial motility during early germination coincided with the induction of mtDNA repair, to ensure that subsequent mixing and redistribution of mtDNA did not involve molecules damaged during drying/imbibition of the seed. We further hypothesized that the massive fusion favored recombination (which may in turn enable recombination-based repair) between mtDNA molecules before partition of the newly organized genome among the newly fragmented mitochondria population. To test these hypotheses, we first quantified total mtDNA during stratification and germination (Figure 9). qPCR of mtDNA relative to nuclear DNA (nucDNA) showed little change in mtDNA copy number during stratification and germination, until a slight increase was detected at the end of germination and during early seedling growth (Figure 9A). A further reduction in relative copy number was measured in 10-d-old seedlings. In contrast, plastic DNA (cpDNA) quantity was unchanged relative to nucDNA during stratification but increased steadily upon transfer to germination-promoting conditions

(Figure 9A). No significant endoreduplication of the nuclear genome occurs in the embryo during stratification, or early germination (Sliwinska et al., 2009), that would affect the relative quantification. However, the increase in mtDNA copy number at the ER, TR, and RH stages may be slightly underestimated due to an increase in ploidy, specifically in the hypocotyl-radicle axis during elongation growth (Sliwinska et al., 2009). We next quantified nucDNA and mtDNA quality by calculating the relative abundance of qPCR amplification of short versus long DNA fragments, on the premise that a relative reduction in long fragment abundance is proportional to DNA damage (Miller-Messmer et al., 2012). No significant change was detected in the relative amplification of long versus short DNA fragments of either nucDNA or mtDNA (Figure 9B). Since mtDNA replication and mtDNA repair are both hypothesized to involve recombination as part of their mechanism, we next chose to investigate recombinational activity of the mtDNA genome. As a first approach, we quantified the relative abundance of recombination-derived products that are known to increase in abundance when control over recombination is relaxed (e.g., in *recA3* and *recG1* mutants). There was no significant increase in recombination products across repeats L or EE during germination, with only repeat EE showing significant increase in recombination in 10-d-old seedlings (Figure 9C). In comparison, mutants defective in suppressing ectopic recombination show greatly increased fold changes in the copy number of these recombination products (Wallet et al., 2015). To confirm the unchanged mtDNA recombination during germination, we next calculated the relative copy number of different regions of the entire mtDNA genome by qPCR using a set of primer pairs spaced between 5 to 10 kb apart (Wallet et al., 2015). We detected no significant changes in stoichiometry of the sequences. Taken together, our results show that the quantity, quality, and recombination/stoichiometry of the mtDNA inherited from the mother, as stored in the seed, are under tight homeostatic control during stratification and germination despite the changes in distribution of the mtDNA nucleoids that takes place during late germination.

DISCUSSION

Promitochondria Bioenergetics Reactivate Immediately upon Imbibition, but Reactivation of Dynamics Only Occurs upon Transfer to Germination Conditions

The term promitochondria has been used as a name for mitochondria in embryos of the dry seed (Logan et al., 2001; Howell et al., 2006) due to their limited internal membrane structure and reduced metabolic activity compared with typical mitochondria seen in most adult plant tissues (compared with promitochondria of yeast; Criddle and Schatz, 1969). However, rather than being nonfunctional scaffolds requiring de novo biogenesis for their activity, promitochondria are specialized for their role in the maintenance of mitochondrial structure and genetic integrity during the challenging periods of maturation drying and seed dormancy. Promitochondria have reduced metabolic activities but are able to generate a membrane potential immediately

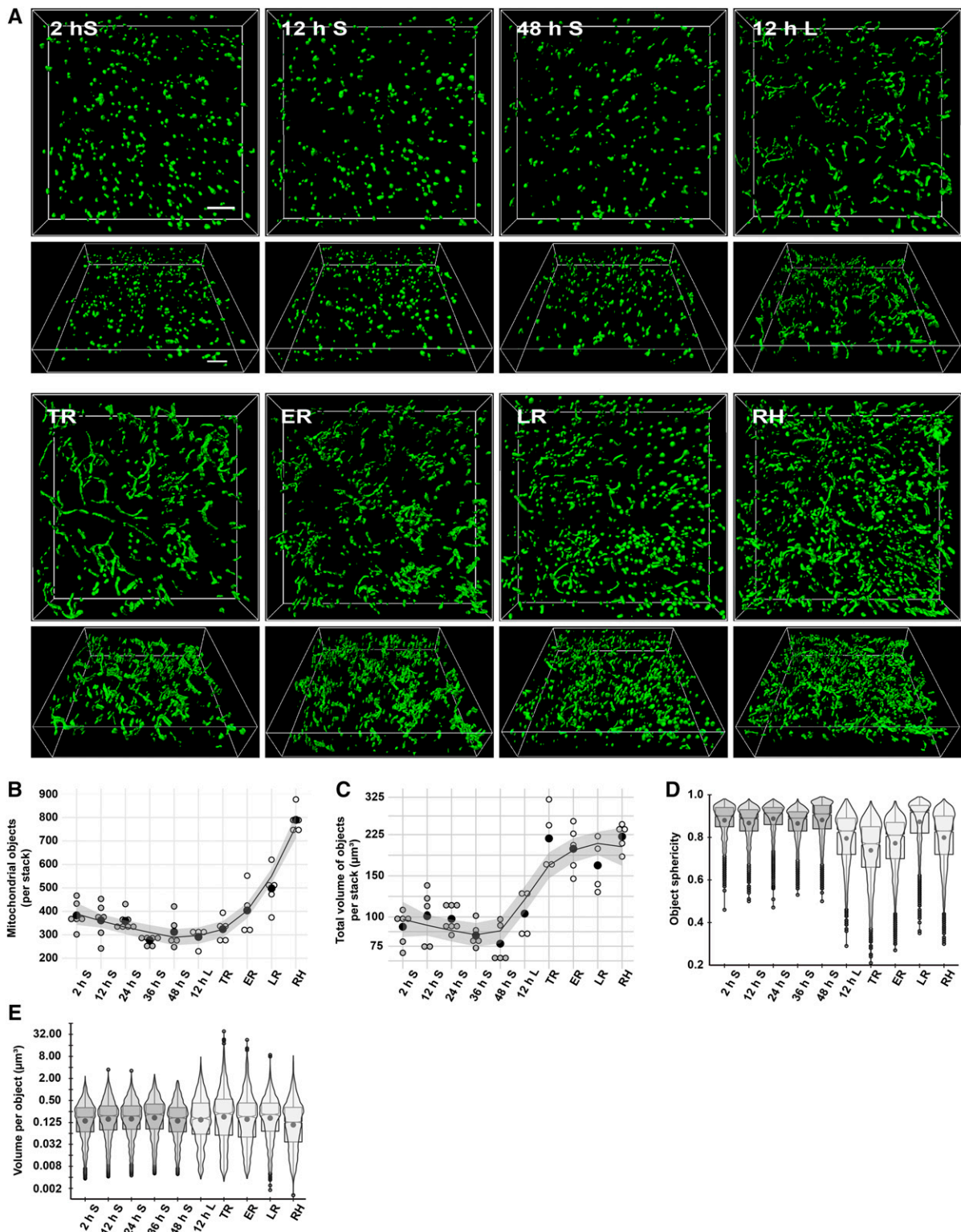


Figure 6. Morphological Changes Affecting the Embryonic Cotyledon Chondriome during Stratification and Germination.

(A) Reconstructed images of CSLM z-stacks of cotyledon mitochondria tagged by mito-GFP. Each image is representative of images captured from at least five seeds at each time point. The bottom image at each time point shows the same z-stack but tilted at -45° relative to the top image. Bars = $5 \mu\text{m}$. See also Supplemental Movie 6.

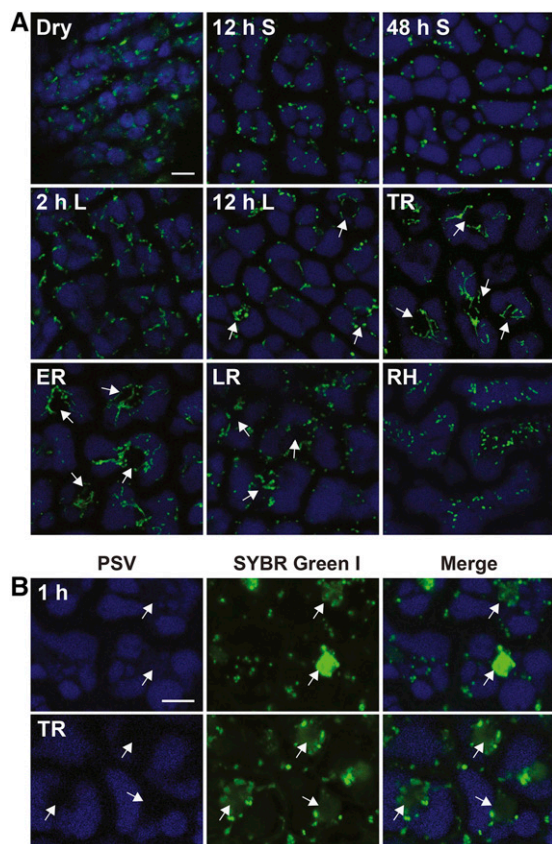


Figure 7. Mitochondria Localize around the Nucleus at the End of Germination.

(A) Visualization of mitochondria (mito-GFP; green) and PSVs (auto-fluorescence; blue) in cotyledon cells observed by CLSM. Arrows indicate PSV-free area. Bar = 5 μm .

(B) Visualization of mtDNA nucleoids and nuclear DNA in Col-0 seed stained with the DNA binding fluorescent dye SYBR Green I. Seed were observed following 1 h of imbibition or during TR stage. The PSV-free area within cells correspond to the position of the SYBR Green I stained nucleus. Arrows indicate PSV-free area/nucleus. Bar = 5 μm .

upon rehydration and can support energy metabolism throughout germination. As such, the initial activation of mitochondrial activity is a biophysical process, controlled principally by hydration status and temperature, rather than a coordinated genetic program controlled by the nucleus.

Promitochondria in the dry seed are immobile due to a lack of hydration, and only local disorganized movement occurs during stratification. However, a massive reactivation of mitochondrial dynamics occurred within 2 h of transfer of stratified seeds to germinating conditions leading to a large increase in intermitochondria interactions (Figure 10). An increase in transcription of nuclear genes encoding proteins involved in import across the outer membrane and in mitochondria transcription and RNA editing accompanies this stage (48 h S/1 h SL) (Law et al., 2012). This reactivation, representing one of the earliest events in the transition from stasis to germination, also occurred in embryos of seed germinating in the absence of stratification, but at a slower rate. The effect of stratification, during which there is limited transcriptional and translational activity of mitochondrial genes (Law et al., 2012), is therefore to synchronize the reactivation across the chondriome. Given that temperature is a key factor controlling the reactivation of mitochondrial dynamics, stratification also acts through inhibition of mitochondrial dynamics until conditions promoting germination are encountered. This inhibition of dynamics may be simply through lower biological activity of the various proteins responsible for mitochondrial dynamics rather than being due to changes in gene expression or protein activity. Increased mitochondrial motility over the next few hours leads to increased fusion concomitant with an increase in mitochondrial membrane biogenesis, with promitochondria acting as scaffolds for the insertion of new polypeptides and lipids (Figure 10). These changes are accompanied with increased transcription at 6 h SL of genes encoding components of the inner membrane import apparatus, protein folding, and mtDNA metabolism (Law et al., 2012).

The modulation of germination by the hormones ABA and GA had little effect on mitochondrial dynamics, reinforcing the view that their reactivation results from the release of biophysical constraints imposed by low tissue hydration and temperature rather than from specific germination cues. ABA, which inhibits germination at the concentration used, reduced the reactivation of mitochondrial dynamics, but only under the germination-promoting conditions of light and 21°C. This suggests there are different requirements for mitochondrial dynamics linked to the two independent programs reported to operate during germination: the ABA-sensitive developmental growth program and the largely ABA-independent storage lipid mobilization program (Pritchard et al., 2002). While temperature is the key trigger for the activation of mitochondrial dynamics, there is clearly a light-mediated effect, which, as

Figure 6. (continued).

(B) Dot plot of the numbers of mitochondrial objects per stack. Open circles indicate total number for each stack while the solid circle indicates the mean. Total number of objects per stack ranges from 1168 to 3954 from at least five seeds per time point. The line represents the Loess regression, while the gray area corresponds to the 95% confidence interval.

(C) Dot plot of the total volume of detected objects per stack, in μm^3 . Open circles indicate the mean chondriome volume per stack, while the solid circle indicates the mean for all stacks. The line represents the Loess regression, while the gray area corresponds to the 95% confidence interval.

(D) Violin box plots of OS (a value of 1 means a perfect sphere). Box plot whiskers indicate $1.5 \times \text{IQR}$, and outliers are represented by an open circle, as described by Tukey. Means are represented by a solid circle. The notch corresponds to the median $\pm 1.58 \times \text{IQR}/\sqrt{n}$.

(E) Violin box plot of the volume per object (in μm^3). Plot design as in **(D)**.

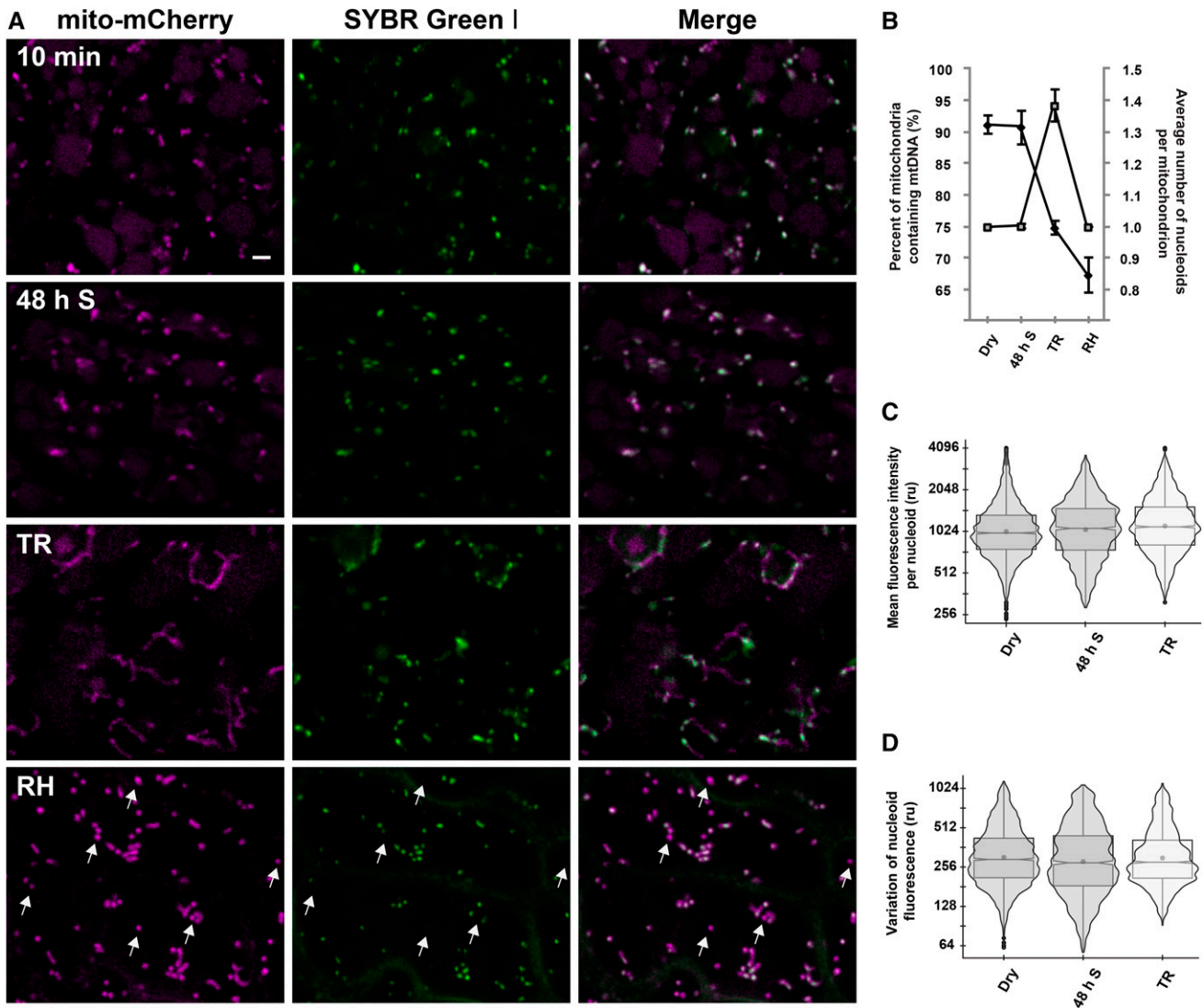


Figure 8. Distribution of mtDNA Nucleoids with the Chondriome of Cotyledon Cells during Stratification and Germination.

(A) Images of mtDNA nucleoids and mitochondria in embryonic cotyledon cells of seed expressing mito-mCherry stained with SYBR Green I. Arrows indicate mitochondria with no apparent SYBR Green I fluorescence. Bars = 5 μ m.

(B) Graph of percentage of mitochondria having a detectable mtDNA nucleoid and of the average nucleoid number per mitochondria (mitochondrial numbers were >1129 and nucleoid numbers >1073 , depending on time point, $n = 7$ seeds).

(C) Violin box plot of the mean fluorescence intensity measured per mtDNA nucleoid in relative units. Box plot whiskers indicate $1.5 \times$ IQR, and any outliers are represented by an open circle, as described by Tukey. Means are represented by a solid circle. The notch corresponds to the median $\pm 1.58 \times$ IQR/ \sqrt{n} .

(D) Violin and box plot of the variation of the fluorescence within each mtDNA nucleoid in relative units. Plot design as in **(C)**.

demonstrated by the effect of paclobutrazol, is linked to the role of light as a germination trigger via a GA-dependent pathway. Mitochondrial dynamics is reduced following paclobutrazol treatment in the light to a similar extent as measured in seed imbibing in the dark at 21°C without stratification. Thus, light triggers the culmination of germination, and this is accompanied by a burst in mitochondrial motility and subsequent intermitochondrial interaction generating the formation of a tubuloreticular chondriome.

Reactivation of Mitochondria Dynamics Leads to the Formation of a Perinuclear Tubuloreticular Structure

The formation of the perinuclear mitochondrial coincides with a massive increase in chondriome volume. Therefore, this change is not simply due to a shift in the fission-fusion balance in favor of a fused state, a conclusion supported by the fact that the number of mitochondria is relatively stable between time of transfer to germination promoting conditions and the TR stage. Instead,

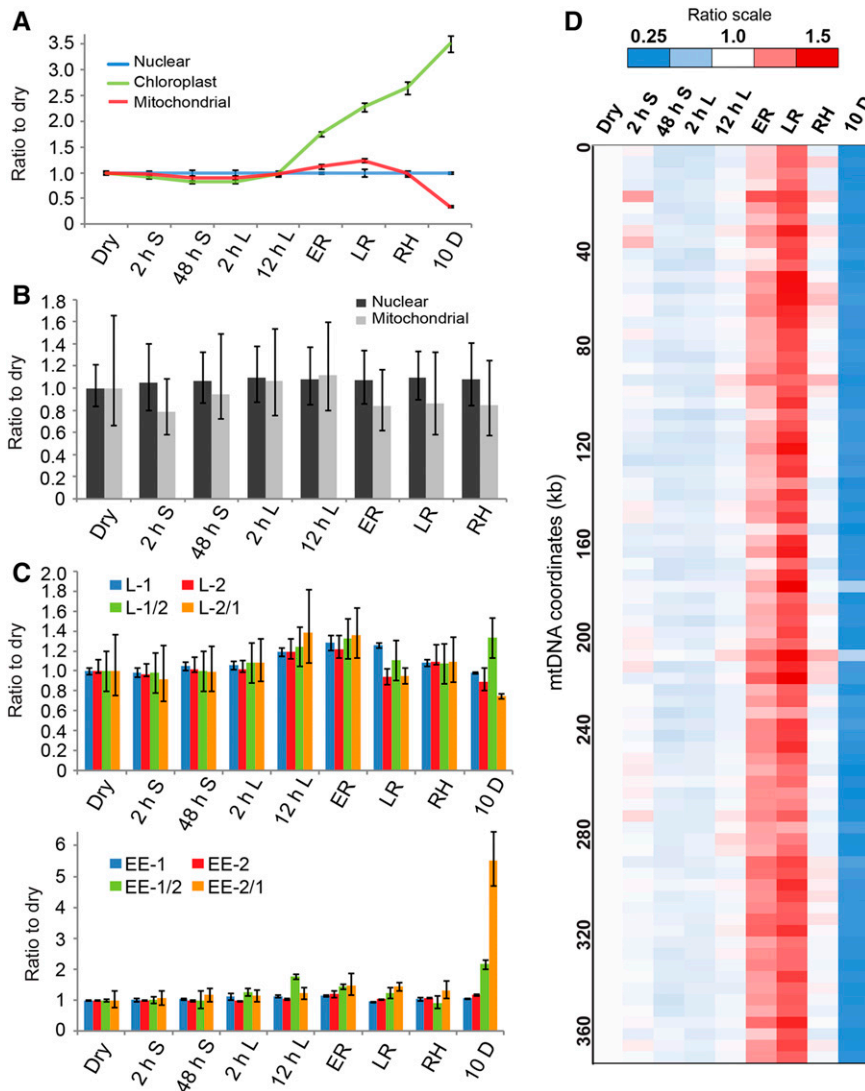


Figure 9. Embryo mtDNA Quantity, Quality, Recombination, and Sequence Stoichiometry Are Tightly Controlled during Germination.

(A) Quantification of the variation in total mtDNA and cpDNA relative copy numbers during stratification, germination, and in 10-d-old seedlings, relative to the dry seed. Values are normalized to nucDNA and presented as means \pm SD of biological duplicates each with three technical replicates.

(B) Quality of mtDNA during germination as detected by qPCR assay. Values represent long PCR fragment abundance relative to that in dry seeds and normalized by the short fragment abundance and relative to amplification of nucDNA targets. Replication as in **(A)**.

(C) qPCR of the accumulation of recombination products across two repeats within the mitochondrial genome. Values indicate the quantity of parental sequence (L-1, L-2, EE-1, and EE-2) or crossover product (L-1/2, L-2/1, EE-1/2, and EE-2/1) relative to in dry seeds for pairs of repeats L and EE. Replication as in **(A)**.

(D) Mitochondrial genome-wide scan for changes in sequences stoichiometry. Sequences spaced 5 to 10 kb apart were quantified by qPCR. Values are relative to the dry seed time point for each PCR product. Replication as in **(A)**.

because there is an increase in chondriome volume while mitochondrial numbers are unchanged, the measured increase in fusion must be balanced by fission and the increase in volume can thus be attributable to a net increase in de novo membrane biogenesis (Figure 10). This increase in membrane biogenesis is a rapid yet transient response to germination triggers leading to a doubling of chondriome volume that is coincident with the second burst of oxygen uptake that occurs during germination

(Sew et al., 2013). While chondriome volume stabilizes at the end of germination, the redifferentiation of promitochondria continues with a peak in abundance at 24/48 h SL of transcripts involved in mitochondrial bioenergetics and metabolism (Law et al., 2012), which is initially coincident with a massive fragmentation of the mitochondrial reticulum leading to a doubling of the number of mitochondria per cell relative to the number before germination was initiated (Figure 10).

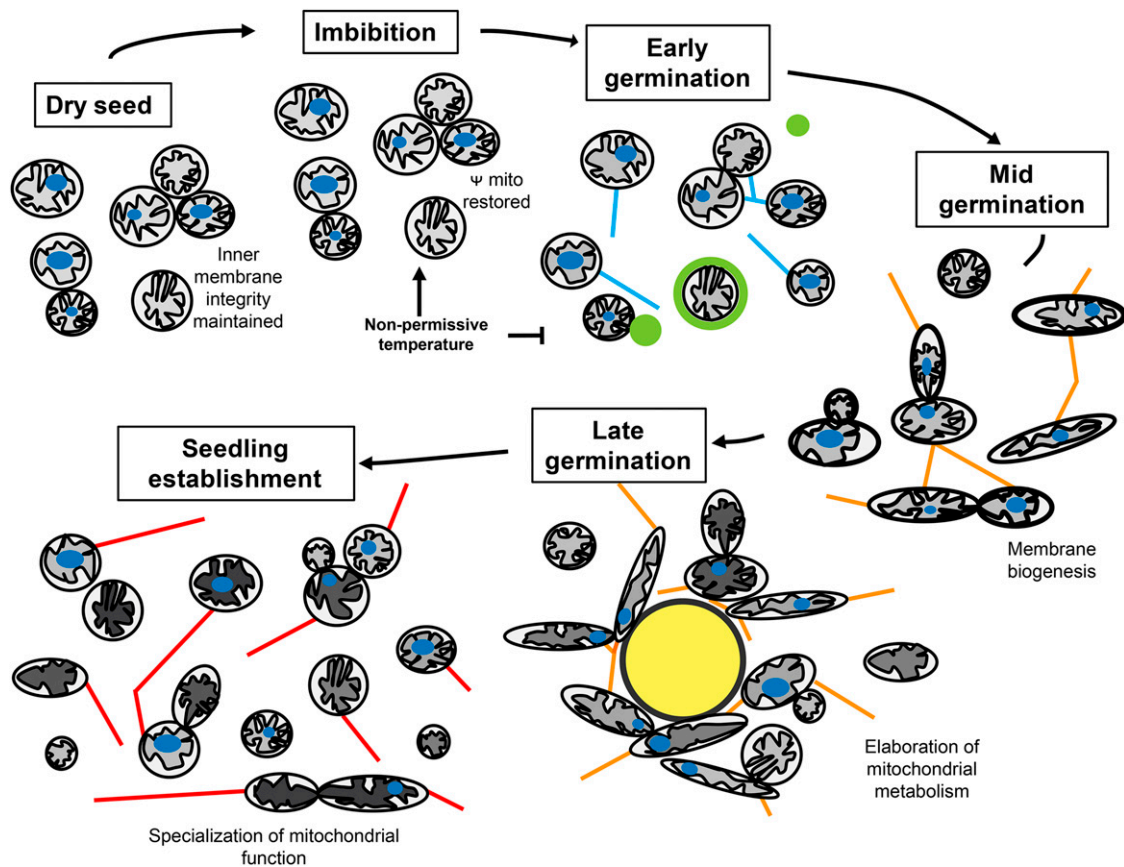


Figure 10. Schematic Representation of Mitochondria Dynamics during Germination.

In dry seed, and during the first hours of imbibition (the first phase of germination), the mitochondria are static and have low metabolic activity despite an immediate reestablishment of a membrane potential. A high percentage of mitochondria contain at least one mtDNA nucleoid. It is proposed that these attributes define these mitochondria as promitochondria and provide a structure and organization that act to minimize damage and thus help ensure mitochondrial quality throughout seed dormancy or quiescence. During the early second phase of germination, initiated upon the transfer of seed to germination promoting conditions, the constraint imposed on mitochondrial dynamics by cold temperature is released leading to a burst of motility, intermitochondrial interactions, and upregulation of mitophagy. During the middle of the second phase of germination, mitochondria become more dynamic, displaying higher rates of intermitochondrial interaction together with a shift to an ovoid morphology. Membrane biogenesis is initiated. At the late second phase of germination, mitochondria are preferentially located around the nucleus and further reticulation and fusion leads to the formation of a perinuclear tubuloreticular mitochondrial structure. This organization may provide a means to ensure mixing of the chondriome and exchange of molecules, together with facilitating synchronization of mitochondrial biogenesis through efficient delivery and import of tRNA and polypeptides encoded by nuclear transcripts and assisting the necessary associated crosstalk between the mitochondrial and nuclear genomes. Following the end of germination, the perinuclear tubuloreticular structure fragments, leading to the reformation of a population of physically discrete mitochondria. The distribution of mtDNA nucleoids among the mitochondria is uneven, indicating division of labor among the physically discrete members of the chondriome. The reorganization of the chondriome, generating an organization typical of more adult tissues, coincides with a burst in mitochondrial metabolic activity as storage reserves are used to fuel postgerminative growth. Blue spots represent mtDNA nucleoids; the nucleus is colored yellow; the matrix is shaded from light to dark gray to indicate increasing bioenergetic activity; increased membrane thickness represents membrane biogenesis; mitochondrial motility is represented by tracks with a scale from blue (slow) to red (fast); nucleation of ATG8 and phagophore formation is indicated in green.

Formation of a mitochondrial cage, encircling the nucleus, has been reported in *Arabidopsis* shoot apical meristem (SAM) and leaf primordia (LP) cells, where cell cycle-dependent changes in chondriome structure lead to the generation of a mitochondrial cage transiently encircling the nucleus (Seguí-Simarro et al., 2008). Similar transient structures have been reported to occur due to massive mitochondrial fusion prior to division of *Arabidopsis*, *Medicago truncatula*, or tobacco protoplasts (Sheahan et al., 2005), and encircling of the nucleus by mitochondria has

been reported to occur during male and female gametogenesis of a number of species (Dickinson and Li, 1988; Nagata, 2003). A perinuclear location has been suggested to facilitate ATP “funneling” to the nucleus during G1/G2 phases of the cell cycle and to the growing spindle and then cell plate at later stages of mitosis and cytokinesis (Seguí-Simarro et al., 2008). However, the tubuloreticular structure at the end of germination is not similarly synchronized with the cell cycle. In the case of the SAM and LP, the cage remained in place during cytokinesis and it was only after cell

division was complete that the chondriome fragmented (Seguí-Simarro et al., 2008). In contrast, in seed cotyledons, formation and fragmentation of the tubuloreticular structure occurred without cell division. Indeed, cell division of *Arabidopsis* cotyledon cells is initiated after protrusion of the radicle, which signals the end of germination (Sliwinska et al., 2009). While ATP provision to the nucleus to support the transcriptional burst concomitant with the end of germination is likely more efficient as a result of a perinuclear location, this location may also facilitate mitochondrial biogenesis through efficient delivery of nuclear-encoded transcripts to ribosomes in the cytosol around the nucleus/perinuclear mitochondria and also import of nuclear synthesized tRNA molecules for mitochondrial translation. For example, mitochondria with a perinuclear location were shown to be enriched in components of the outer membrane protein import apparatus, relative to mitochondria in the cell periphery of cultured mammalian cells (Wurm et al., 2011). In addition, and as suggested by Seguí-Simarro et al. (2008) in the case of SAM and LP cells, the formation of a cage-like mitochondrial reticulum provides conditions for intermixing of, and recombination between, the population of mtDNA molecules of different sizes and compositions that comprise the mitochondrial genome. Mitochondrial genome continuity in the new generation is then ensured by redistribution of the homogenized genome throughout the mitochondrial population of the daughter cells following division of the fused chondriome (Seguí-Simarro et al., 2008). While reorganization of the chondriome during germination enables homogenization of the mtDNA, subsequent fragmentation at the end of germination generates a population of discrete mitochondria with heterogeneous, rather than homogeneous, mtDNA content, in contrast to the situation with dividing protoplasts (Sheahan et al., 2007, 2005); the distribution of nucleoids in SAM and LP cells before and after cage formation has not been reported. A heterogeneous distribution of mtDNA within the physically discrete mitochondria is typical of plant cells (Sheahan et al., 2005; Arimura et al., 2004; Lonsdale et al., 1988; Logan, 2006; Satoh et al., 1993; Preuten et al., 2010) and led to the plant chondriome being termed a discontinuous whole (Logan, 2006). This heterogeneity is evidence of division of labor between members of the chondriome, with some mitochondria probably functioning as “genetic vaults” designed to protect vital genetic material (Logan, 2006).

Promitochondria Are Specialized Transgenerational Genetic Vaults That Redifferentiate during Germination for Autotrophic Growth

All promitochondria are specialized as genetic vaults rather than being degradation products or structures requiring biogenesis in order to assume function: Over 90% contain a visible mtDNA nucleoid, recombination is under tight control in order to maintain structural integrity, mtDNA replication is tightly coupled to that of the nuclear DNA, and they can fuel energy metabolism, relying on metabolites accumulated during maturation (Fait et al., 2006). These characteristics enable promitochondria to faithfully fulfill their role in maintaining the integrity of the mitochondrial genome during embryo maturation, imbibition, and germination, which in turn ensures continuation of the species. The fact that mito-GFP is readily detected in dry seeds provides additional evidence that

promitochondria are protected. In addition, the lack of mitochondrial motility even when the actin cytoskeleton is present and dynamic may help ensure safe storage of the mtDNA within each discrete compartment. Such a role for promitochondria is in agreement with the results of Law et al. (2012) that showed relatively low transcript abundances for genes involved in mitochondrial biogenesis during stratification, before a transient increase in abundance upon transfer to germination promoting conditions, which precedes the doubling of mitochondrial volume as promitochondria are used as a scaffold for the incorporation of new membrane lipids and proteins.

Thus, promitochondria are apparently specialized for specific roles, but even within the promitochondrial population there is evidence of further division of labor. The reactivation of mitochondria after transfer to germinating-promoting conditions is heterogeneous, with some organelles becoming mobile after only a few minutes of observation. These “first responders” then interact/fuse with nearby partners before the wave of interaction spreads to more distant mitochondria. At the same time, there are other mitochondria that display no organized movement and do not interact with others. The violin plots of rates of fusion and numbers of interactors clearly show the existence of such subpopulations. One possibility is that these singleton mitochondria are specialized for tasks that do not require them to fuse, or they may be isolated from the rest of the chondriome due to dysfunction, perhaps an inability to fuse, and instead these mitochondria may be the targets for the measured upregulation of mitophagy following initiation of germination. However, the clearest indicator of division of labor is the increase in the percentage of mitochondria with no visible nucleoid following fragmentation of the perinuclear tubuloreticular structure, a condition maintained in seedling tissue (Preuten et al., 2010). This heterogeneity is generated simultaneously with the doubling of mitochondrial volume and number and precedes a boost in mitochondrial dynamics in the newly germinated seedling and the coincident increased respiratory activity that fuels seedling growth and development (Figure 10). It is hypothesized that biogenesis is tailored to the generation of mitochondria specialized for energy production alongside mitochondria with other functions (for example, as genetic vaults) rather than a uniform rebuilding of all promitochondria to enable full mitochondrial functionality. Concomitant with this hypothetical phase of specialization of mitochondrial functions was the uncoupling of mtDNA replication from that of the nuclear genome and a relaxing of control over mtDNA recombination. Taken together, these discoveries indicate that mitochondrial specialization is a highly orchestrated event in the transition from heterotrophic growth during germination to autotrophy in the developing seedling.

METHODS

Plants Materials and Growth Conditions

All experiments were performed using the *Arabidopsis thaliana* Columbia ecotype (Col-0). Visualization of mitochondria was performed using transgenic lines expressing mGFP5 (Siemering et al., 1996) or mCherry (Shaner et al., 2004) targeted to the mitochondrial matrix (mito-GFP [Logan and Leaver, 2000] or mito-mCherry [Candat et al., 2014]). In order to

visualize actin filaments and mitochondria, a double transgenic line was used expressing mito-GFP and an in-frame fusion of mCherry to the actin binding domain of mouse talin (El Zawily et al., 2014; Kost et al., 1998). The endoplasmic reticulum was observed in a line expressing YFP-HDEL (Saint-Jore et al., 2002; Teh and Moore, 2007), while peroxisomes were observed in a line expressing YFP-SKL (Mathur et al., 2002). To visualize autophagosomes and mitochondria, the mito-GFP line (kanamycin resistant) was retransformed with a construct containing mRFP1-ATG8F under the control of the 35S promoter in a binary plasmid conferring resistance to BASTA (Honig et al., 2012). Double transgenics were selected by BASTA resistance and by microscopy. All lines were used within 6 months of harvest and seeds stored over desiccant at -20°C . Seeds were surface sterilized in the dark by washing in 80% (v/v) ethanol and then in 30% (v/v) household bleach for 5 min with continual inversion, followed by three rinses in sterile water. Sterilized seeds were immediately spread on a nitrocellulose membrane (Sartorius) over two circles of Whatman No. 1 filter paper in 47-mm glass Petri dish. Dishes were wrapped in aluminum foil and transferred to 4°C in the dark for stratification. After 48 h, the plates were unwrapped and transferred to a growth chamber at 21°C under continuous cool-white light ($50\ \mu\text{mol m}^{-2}\ \text{s}^{-1}$). For treatment with $100\ \mu\text{M}$ ABA (Sigma-Aldrich), $100\ \mu\text{M}$ GA_3 (Sigma-Aldrich), or $100\ \mu\text{M}$ paclobutrazol (Riedel-de Haen), seed were incubated in test or control solutions from the start of imbibition and throughout the germination time course. Drug concentrations were chosen to saturate the responses as determined in previous studies (Debeaujon et al., 2000; Müller et al., 2006).

Live-Cell Imaging

Observation of dry embryos was performed after applying gentle pressure on seeds held between two glass microscope slides in order to break the testa and endosperm tissues and gain visible access to the embryonic tissues. During stratification and germination time courses, embryos were carefully removed from the testa and endosperm by the application of gentle pressure to seeds in water between microscope slide and cover slip. All tissue was mounted in perfluorodecalin (octadecafluorodecahydronaphtalene; Fluka) (Littlejohn et al., 2010). For all experiments, each image stack corresponds to a different embryo. Live-cell CLSM was performed using a Nikon A1 microscope driven by NIS Elements software (Nikon) using Nikon $40\times$ CFI Plan Apochromat oil-immersion objective (NA 1.3) or $60\times$ CFI Plan Apochromat oil immersion objective (NA 1.4) for experiments using SYBR Green I. Excitation and emission wavelengths for the different probes were as follows: mito-GFP/SYBR Green I/YFP, 488/500 to 550 nm; mCherry/mRFP1/TMRM, 561/570 to 620 nm; and PSV autofluorescence, 405/425 to 475 nm. Dichroic mirrors of 405/488 or 405/488/561 were used as appropriate. Live imaging, using line switching between channels, was performed on the same area of embryonic cotyledons of between 5 and 11 different seeds from at least two independent experiments per time point and/or per condition.

Quantification of Mitochondria Morphologies

Z-stacks were captured first at 2 h from the start of imbibition (stratification) and then at 12-h intervals up to 60 h. In addition, stacks were captured of the four late germination and postgermination stages of TR, ER, LR, and RH. Stacks of slices $37.29 \times 37.29\ \mu\text{m}$ with a z-step of $0.15\ \mu\text{m}$ were captured at an image size of 1024×1024 pixels with a pixel size of $0.04\ \mu\text{m}$ and pixel dwell time of $1.2\ \mu\text{s}$. The z-stacks were then reconstructed using IMARIS v7 (Bitplane). Object reconstructions were performed by automatic thresholding using background subtraction (rolling ball of $0.273\ \mu\text{m}$). The parameters measured to describe the 3D reconstruction are as follows: objects numbers (object per stacks) or volume (in relative unit, per object or total) and sphericity (0 to 1 unit, per object). Data were then exported to R (R Core Team, 2013) to perform statistical analysis. To facilitate

visualization, the distribution of object volume is presented on logarithmic scale (base 2), while object numbers and sphericity are on linear scales.

Quantification of Organelle Dynamics

Stacks of images, 37.29×37.29 , were captured at 15.47-s intervals for 5 min 15 s, with an image size of 2048×2048 pixels, giving a pixel size of $0.02\ \mu\text{m}$. Stacks were processed using IMARIS v7 to enable object identification, tracking, and the calculation of various dynamics parameters. Object reconstructions were performed by automatic thresholding using background subtraction (rolling ball of $0.237\ \mu\text{m}$). Tracking over time was performed using the connected component algorithm. Parameters measured were mean track speed, track displacement, track straightness (relative unit from 0 to 1), total number of interactions with other mitochondria, fusion rate per mitochondria for mitochondria interacting at least once, and the percentage of mitochondria interacting at least once. Peroxisome movement was also quantified by ImarisTrack. Endoplasmic reticulum time stacks were processed using Fiji (Schindelin et al., 2012) to filter noise and to superimpose two images ($25 \times 25\ \mu\text{m}$) of the same field of view captured 309 s apart. Colocalization analysis of these two images was performed with the Coloc 2 plug-in using the Costes method (Costes et al., 2004). Following stratification for 48 h, plates were transferred to light/ 21°C or dark/ 21°C for 2 h. Image capture was performed within 30 min of opening the plate. Statistical analysis was performed using R. Track-derived parameter measurements were weighted to account for number of mitochondria per track to avoid underestimation resulting from track sharing.

TMRM Staining

The ability of mitochondria to generate a membrane potential was determined *in vivo* by the observation of the fluorescent dye TMRM, which accumulates in mitochondria in a potentiometric manner (Brand and Nicholls, 2011). Dry mito-GFP seed were incubated under gentle vacuum in freshly prepared 50 nM TMRM for 10 min before dissection. Dissected embryos were mounted in 50 nM TMRM, and image capture (image size 2048×2048 pixels covering an area of $125.88 \times 125.88\ \mu\text{m}$ with a pixel size of $0.06\ \mu\text{m}$) by CSLM was achieved within a further 5 min. Colocalization analysis of the TMRM and GFP fluorescence signal was performed on regions of interest of $50 \times 50\ \mu\text{m}$ in Fiji using the Coloc2 plug-in. The Mander's coefficient was chosen in order to calculate the percentage of pixels registering mito-GFP that also register TMRM fluorescence. Statistical analysis was performed using R.

Respiration Measurement

Oxygen consumption of seeds was measured in 1 mL of deionized water with a liquid-phase Oxytherm oxygen electrode system (Hansatech) calibrated at the measurement temperature. Dry seeds (20–40 mg dry weight) were directly imbibed in the electrode chamber. For experiments with stratified seeds (48 h, 4°C in the dark), seeds (20–40 mg dry weight) were transferred to the electrode chamber for measurements at 4°C or after 2 h of incubation at 21°C in the light ($50\ \mu\text{mol m}^{-2}\ \text{s}^{-1}$) for measurements at 21°C . To estimate capacity of the alternative pathway, O_2 consumption rate was measured after addition of $500\ \mu\text{M}$ KCN.

Actin Imaging

Image capture of actin dynamics was performed at an image size of 2048×2048 pixels (line averaging of 4), with a pixel size of $0.04\ \mu\text{m}$ covering an area of $81.6 \times 81.6\ \mu\text{m}$. Movies were captured at a frame rate of 1 per 92 s over a recording period of 369 s. Images were imported to Fiji where they were cropped to $20 \times 20\ \mu\text{m}$ and processed to reduce noise by applying Gaussian blur.

SYBR Green I Staining

SYBR Green I (Thermo Scientific) is a cell-permeable dye that binds preferentially to double-stranded DNA and then emits green fluorescence under blue light excitation. To enable visualization of mtDNA and mitochondria, we used seed from a transgenic *Arabidopsis* line expressing matrix targeted mCherry (Candat et al., 2014) stained with SYBR Green I at a dilution of 1:10,000. For the 10 min time point, dry seed was incubated in SYBR Green I for 10 min with gentle vacuum before the embryo was carefully dissected from the surrounding tissues. For later time points, embryos were first dissected from seed imbibed for the appropriate time before. Each image, $66.88 \times 66.88 \mu\text{m}$, was captured from a different embryo ($n = 7$) and was captured at 2048 pixels, with a pixel size of $0.03 \mu\text{m}$. Stacks were processed using IMARIS v7 using the same thresholding for all images. Object reconstructions were performed by automatic absolute thresholding. Parameters measured were number of mitochondria, number of mitochondria with mtDNA, the numbers of mtDNA nucleoid, the nucleoid plan area (μm^2), the nucleoid relative fluorescence (relative unit), and the spatial variation of fluorescence within the nucleoid. Statistical significance testing was performed by ANOVA.

qPCR Analysis

qPCR assays were performed in a LightCycler480 (Roche), in $6 \mu\text{L}$ of reaction containing $1 \times$ LightCycler 480SYBR Green I Master (Roche) and $0.5 \mu\text{M}$ each primer, except for DNA quality assays. The thermocycling program was as follows: 7 min denaturing step at 95°C , 40 cycles of 10 s at 95°C , 15 s at 58°C , and 15 s at 72°C . The second derivative maximum method was used to determine C_p values, and PCR efficiencies were determined from DNA serial dilution curves or using LinRegPCR software (<http://LinRegPCR.nl>). Three technical replicates were performed for each experiment. The numbers of biological replicates are indicated in the figures. For quantification of mtDNA and cpDNA copy numbers, a set of primers located along the organellar genomes was used, and results were normalized against the *UBQ10* (At4g05320) and *ACT1* (At2g37620) nuclear genes. The same method was used to record mtDNA stoichiometry (Wallet et al., 2015). To measure the accumulation of ectopic recombination in mtDNA, primers flanking repeat R15 and R26 were used (Wallet et al., 2015). The *COX2* (AtMG00160) and 18S rRNA (AtMG01390) mitochondrial genes were used for normalization. DNA quality assays were performed in a LightCycler CFX96 (Bio-Rad), in $10 \mu\text{L}$ of reaction containing $1 \times$ SSoAdvanced Universal SYBR Green SuperMix (Bio-Rad) and $0.5 \mu\text{M}$ each primer. The thermocycling program was as follows: 7 min denaturing step at 95°C , then 40 cycles of 10 s at 95°C and 45 s at 60°C . To quantify DNA quality, sets of primers were used to amplify either long fragments or short fragments of the mitochondrial or nuclear genomes as described by Miller-Messmer et al. (2012).

Accession Numbers

Sequence data from this article can be found in the *Arabidopsis* Genome Initiative or GenBank/EMBL databases under the following accession numbers: *ACT1* (At2g37620), *ATG8F* (At4g16520), *COX2* (AtMG00160), *UBQ10* (At4g05320), and 18S rRNA (AtMG01390).

Supplemental Data

Supplemental Figure 1. Mitochondrial dynamics in cells of green cotyledons at 4 d postgermination.

Supplemental Figure 2. Reactivation of dynamics of cotyledon mitochondria is delayed without stratification but displays a similar profile.

Supplemental Results. Dynamics of mitochondria in mature green cotyledons and dynamics with no stratification.

Supplemental Movie 1. Immobile mitochondria in dry seed and tracking of motile mitochondria during germination.

Supplemental Movie 2. Tracking of mitochondria in seed without stratification.

Supplemental Movie 3. F-actin and mitochondrial dynamics in stratifying seed.

Supplemental Movie 4. ATG8F bodies associate with mitochondria.

Supplemental Movie 5. ATG8F bodies seen encapsulating mitochondria.

Supplemental Movie 6. Rendered Z-stacks of cotyledon mitochondria during germination.

Supplemental Movie 7. Dynamics of mitochondria and mtDNA nucleoids at the TR stage.

ACKNOWLEDGMENTS

We thank Fabienne Simonneau and Mayeul Millien of the IMAC imaging plateau SFR QUASAV; the University of Angers for the doctoral contract "Président" awarded to G.P.; Jaideep Mathur (University of Guelph) for the YFP-SKL construct; Ian Moore (University of Oxford) for YFP-HDEL; and Gad Galili for the mRFP1-ATG8F construct. We also thank Martine Neveu for taking care of plant lines in Angers and Aurélie Rolland for her qPCR expertise.

AUTHOR CONTRIBUTIONS

G.P. and D.C.L. conceived the project and designed the experiments. G.P. performed all microscopy and genome copy number/repair qPCR. G.P. and D.C.L. made the mito-GFP mRFP1-ATG8F double transgenics. J.M.G. performed the qPCR analysis of mitochondrial sequences stoichiometry and analyzed the data. A.B. and D.M. performed respiration measurements and analyzed the data. G.P. and D.C.L. wrote the manuscript with additions and revisions by J.M.G. and D.M.

Received September 13, 2016; revised December 6, 2016; accepted January 6, 2017; published January 6, 2017.

REFERENCES

- Arimura, S., Yamamoto, J., Aida, G.P., Nakazono, M., and Tsutsumi, N. (2004). Frequent fusion and fission of plant mitochondria with unequal nucleoid distribution. *Proc. Natl. Acad. Sci. USA* **101**: 7805–7808.
- Atkin, O.K., and Tjoelker, M.G. (2003). Thermal acclimation and the dynamic response of plant respiration to temperature. *Trends Plant Sci.* **8**: 343–351.
- Attucci, S., Carde, J.P., Raymond, P., Saint-Gès, V., Spiteri, A., and Pradet, A. (1991). Oxidative phosphorylation by mitochondria extracted from dry sunflower seeds. *Plant Physiol.* **95**: 390–398.
- Baskin, C.C., and Baskin, J.M. (2014). *Seeds: Ecology, Biogeography, and Evolution of Dormancy and Germination*. (Cambridge, MA: Academic Press).
- Benamar, A., Tallon, C., and Macherel, D. (2003). Membrane integrity and oxidative properties of mitochondria isolated from imbibing pea seeds after priming or accelerated ageing. *Seed Sci. Res.* **13**: 35–45.

- Bolte, S., Lanquar, V., Soler, M.-N., Beebo, A., Satiat-Jeuenaître, B., Bouhidel, K., and Thomine, S.** (2011). Distinct lytic vacuolar compartments are embedded inside the protein storage vacuole of dry and germinating *Arabidopsis thaliana* seeds. *Plant Cell Physiol.* **52**: 1142–1152.
- Brand, M.D., and Nicholls, D.G.** (2011). Assessing mitochondrial dysfunction in cells. *Biochem. J.* **435**: 297–312.
- Candat, A., Paszkiewicz, G., Neveu, M., Gautier, R., Logan, D.C., Avelange-Macherel, M.-H., and Macherel, D.** (2014). The ubiquitous distribution of late embryogenesis abundant proteins across cell compartments in *Arabidopsis* offers tailored protection against abiotic stress. *Plant Cell* **26**: 3148–3166.
- Carrie, C., Murcha, M.W., Millar, A.H., Smith, S.M., and Whelan, J.** (2007). Nine 3-ketoacyl-CoA thiolases (KATs) and acetoacetyl-CoA thiolases (ACATs) encoded by five genes in *Arabidopsis thaliana* are targeted either to peroxisomes or cytosol but not to mitochondria. *Plant Mol. Biol.* **63**: 97–108.
- Costes, S.V., Daelemans, D., Cho, E.H., Dobbin, Z., Pavlakis, G., and Lockett, S.** (2004). Automatic and quantitative measurement of protein-protein colocalization in live cells. *Biophys. J.* **86**: 3993–4003.
- Criddle, R.S., and Schatz, G.** (1969). Promitochondria of anaerobically grown yeast. I. Isolation and biochemical properties. *Biochemistry* **8**: 322–334.
- Dai, H., Lo, Y.-S., Jane, W.-N., Lee, L.-W., and Chiang, K.-S.** (1998). Population heterogeneity of higher-plant mitochondria in structure and function. *Eur. J. Cell Biol.* **75**: 198–209.
- Debeaujon, I., Léon-Kloosterziel, K.M., and Koornneef, M.** (2000). Influence of the testa on seed dormancy, germination, and longevity in *Arabidopsis*. *Plant Physiol.* **122**: 403–414.
- Dickinson, H.G., and Li, F.L.** (1988). Organelle behaviour during gametogenesis. In *Division and Segregation of Organelles*, and S.A. Boffey and D. Lloyd, eds (Cambridge, UK: Cambridge University Press), pp. 131–148.
- Ehrenshaft, M., and Brambl, R.** (1990). Respiration and mitochondrial biogenesis in germinating embryos of maize. *Plant Physiol.* **93**: 295–304.
- El Zawily, A.M., et al.** (2014). FRIENDLY regulates mitochondrial distribution, fusion, and quality control in *Arabidopsis*. *Plant Physiol.* **166**: 808–828.
- Fait, A., Angelovici, R., Less, H., Ohad, I., Urbanczyk-Wochniak, E., Fernie, A.R., and Galili, G.** (2006). *Arabidopsis* seed development and germination is associated with temporally distinct metabolic switches. *Plant Physiol.* **142**: 839–854.
- Finkelstein, R., Reeves, W., Ariizumi, T., and Steber, C.** (2008). Molecular aspects of seed dormancy. *Annu. Rev. Plant Biol.* **59**: 387–415.
- Fuji, K., Shimada, T., Takahashi, H., Tamura, K., Koumoto, Y., Utsumi, S., Nishizawa, K., Maruyama, N., and Hara-Nishimura, I.** (2007). *Arabidopsis* vacuolar sorting mutants (green fluorescent seed) can be identified efficiently by secretion of vacuole-targeted green fluorescent protein in their seeds. *Plant Cell* **19**: 597–609.
- Honig, A., Avin-Wittenberg, T., Ufaz, S., and Galili, G.** (2012). A new type of compartment, defined by plant-specific Atg8-interacting proteins, is induced upon exposure of *Arabidopsis* plants to carbon starvation. *Plant Cell* **24**: 288–303.
- Howell, K.A., Millar, A.H., and Whelan, J.** (2006). Ordered assembly of mitochondria during rice germination begins with pro-mitochondrial structures rich in components of the protein import apparatus. *Plant Mol. Biol.* **60**: 201–223.
- Hunter, P.R., Craddock, C.P., Di Benedetto, S., Roberts, L.M., and Frigerio, L.** (2007). Fluorescent reporter proteins for the tonoplast and the vacuolar lumen identify a single vacuolar compartment in *Arabidopsis* cells. *Plant Physiol.* **145**: 1371–1382.
- Jedd, G., and Chua, N.H.** (2002). Visualization of peroxisomes in living plant cells reveals acto-myosin-dependent cytoplasmic streaming and peroxisome budding. *Plant Cell Physiol.* **43**: 384–392.
- Kost, B., Spielhofer, P., and Chua, N.H.** (1998). A GFP-mouse talin fusion protein labels plant actin filaments in vivo and visualizes the actin cytoskeleton in growing pollen tubes. *Plant J.* **16**: 393–401.
- Law, S.R., Narsai, R., Taylor, N.L., Delannoy, E., Carrie, C., Giraud, E., Millar, A.H., Small, I., and Whelan, J.** (2012). Nucleotide and RNA metabolism prime translational initiation in the earliest events of mitochondrial biogenesis during *Arabidopsis* germination. *Plant Physiol.* **158**: 1610–1627.
- Littlejohn, G.R., Gouveia, J.D., Edner, C., Smirnov, N., and Love, J.** (2010). Perfluorodecalin enhances in vivo confocal microscopy resolution of *Arabidopsis thaliana* mesophyll. *New Phytol.* **186**: 1018–1025.
- Liu, P.P., Koizuka, N., Homrichhausen, T.M., Hewitt, J.R., Martin, R.C., and Nonogaki, H.** (2005). Large-scale screening of *Arabidopsis* enhancer-trap lines for seed germination-associated genes. *Plant J.* **41**: 936–944.
- Logan, D.C.** (2006). The mitochondrial compartment. *J. Exp. Bot.* **57**: 1225–1243.
- Logan, D.C., and Leaver, C.J.** (2000). Mitochondria-targeted GFP highlights the heterogeneity of mitochondrial shape, size and movement within living plant cells. *J. Exp. Bot.* **51**: 865–871.
- Logan, D.C., Millar, A.H., Sweetlove, L.J., Hill, S.A., and Leaver, C.J.** (2001). Mitochondrial biogenesis during germination in maize embryos. *Plant Physiol.* **125**: 662–672.
- Lonsdale, D.M., Brears, T., Hodge, T.P., Melville, S.E., and Rottmann, W.H.** (1988). The plant mitochondrial genome: Homologous recombination as a mechanism for generating heterogeneity. *Philos. Trans. R. Soc. London Ser. B Biol. Sci.* **319**: 149–163.
- Mathur, J., Mathur, N., and Hülskamp, M.** (2002). Simultaneous visualization of peroxisomes and cytoskeletal elements reveals actin and not microtubule-based peroxisome motility in plants. *Plant Physiol.* **128**: 1031–1045.
- Miller-Messmer, M., Kühn, K., Bichara, M., Le Ret, M., Imbault, P., and Gualberto, J.M.** (2012). RecA-dependent DNA repair results in increased heteroplasmy of the *Arabidopsis* mitochondrial genome. *Plant Physiol.* **159**: 211–226.
- Müller, K., Tintelnot, S., and Leubner-Metzger, G.** (2006). Endosperm-limited Brassicaceae seed germination: abscisic acid inhibits embryo-induced endosperm weakening of *Lepidium sativum* (cress) and endosperm rupture of cress and *Arabidopsis thaliana*. *Plant Cell Physiol.* **47**: 864–877.
- Nagata, N.** (2003). Differentiation of organelles during male gametophyte development in higher plants. *Plant Morphol.* **15**: 68–75.
- Narsai, R., Law, S.R., Carrie, C., Xu, L., and Whelan, J.** (2011a). In-depth temporal transcriptome profiling reveals a crucial developmental switch with roles for RNA processing and organelle metabolism that are essential for germination in *Arabidopsis*. *Plant Physiol.* **157**: 1342–1362.
- Preston, C.** (2009). *Thomas Browne and the Writing of Early Modern Science*. (Cambridge, UK: Cambridge University Press).
- Preuten, T., Cincu, E., Fuchs, J., Zoschke, R., Liere, K., and Börner, T.** (2010). Fewer genes than organelles: extremely low and variable gene copy numbers in mitochondria of somatic plant cells. *Plant J.* **64**: 948–959.
- Pritchard, S.L., Charlton, W.L., Baker, A., and Graham, I.A.** (2002). Germination and storage reserve mobilization are regulated independently in *Arabidopsis*. *Plant J.* **31**: 639–647.
- R Core Team** (2013). *R: A Language and Environment for Statistical Computing*. (Vienna, Austria: R Foundation for Statistical Computing).

- Saint-Jore, C.M., Evins, J., Batoko, H., Brandizzi, F., Moore, I., and Hawes, C.** (2002). Redistribution of membrane proteins between the Golgi apparatus and endoplasmic reticulum in plants is reversible and not dependent on cytoskeletal networks. *Plant J.* **29**: 661–678.
- Satoh, M., Nemoto, Y., Kawano, S., Nagata, T., Hirokawa, H., and Kuroiwa, T.** (1993). Organization of heterogeneous mitochondrial DNA molecules in mitochondrial nuclei of cultured tobacco cells. *Protoplasma* **175**: 112–120.
- Schindelin, J., et al.** (2012). Fiji: an open-source platform for biological-image analysis. *Nat. Methods* **9**: 676–682.
- Seguí-Simarro, J.M., Coronado, M.J., and Staehelin, L.A.** (2008). The mitochondrial cycle of *Arabidopsis* shoot apical meristem and leaf primordium meristematic cells is defined by a perinuclear tentaculate/cage-like mitochondrion. *Plant Physiol.* **148**: 1380–1393.
- Sew, Y.S., Ströher, E., Holzmann, C., Huang, S., Taylor, N.L., Jordana, X., and Millar, A.H.** (2013). Multiplex micro-respiratory measurements of *Arabidopsis* tissues. *New Phytol.* **200**: 922–932.
- Shaner, N.C., Campbell, R.E., Steinbach, P.A., Giepmans, B.N.G., Palmer, A.E., and Tsien, R.Y.** (2004). Improved monomeric red, orange and yellow fluorescent proteins derived from *Discosoma* sp. red fluorescent protein. *Nat. Biotechnol.* **22**: 1567–1572.
- Sheahan, M.B., McCurdy, D.W., and Rose, R.J.** (2005). Mitochondria as a connected population: ensuring continuity of the mitochondrial genome during plant cell dedifferentiation through massive mitochondrial fusion. *Plant J.* **44**: 744–755.
- Sheahan, M.B., Rose, R.J., and McCurdy, D.W.** (2007). Mechanisms of organelle inheritance in dividing plant cells. *J. Integr. Plant Biol.* **49**: 1208–1218.
- Siemering, K.R., Golbik, R., Sever, R., and Haseloff, J.** (1996). Mutations that suppress the thermosensitivity of green fluorescent protein. *Curr. Biol.* **6**: 1653–1663.
- Sliwiska, E., Bassel, G.W., and Bewley, J.D.** (2009). Germination of *Arabidopsis thaliana* seeds is not completed as a result of elongation of the radicle but of the adjacent transition zone and lower hypocotyl. *J. Exp. Bot.* **60**: 3587–3594.
- Teh, O.-K., and Moore, I.** (2007). An ARF-GEF acting at the Golgi and in selective endocytosis in polarized plant cells. *Nature* **448**: 493–496.
- Ueda, H., Yokota, E., Kutsuna, N., Shimada, T., Tamura, K., Shimmen, T., Hasezawa, S., Dolja, V.V., and Hara-Nishimura, I.** (2010). Myosin-dependent endoplasmic reticulum motility and F-actin organization in plant cells. *Proc. Natl. Acad. Sci. USA* **107**: 6894–6899.
- Wallet, C., Le Ret, M., Bergdoll, M., Bichara, M., Dietrich, A., and Gualberto, J.M.** (2015). The RECG1 DNA translocase is a key factor in recombination surveillance, repair, and segregation of the mitochondrial DNA in *Arabidopsis*. *Plant Cell* **27**: 2907–2925.
- Wang, J., Rajakulendran, N., Amirsadeghi, S., and Vanlerberghe, G.C.** (2011). Impact of mitochondrial alternative oxidase expression on the response of *Nicotiana tabacum* to cold temperature. *Physiol. Plant.* **142**: 339–351.
- Wurm, C.A., Neumann, D., Lauterbach, M.A., Harke, B., Egner, A., Hell, S.W., and Jakobs, S.** (2011). Nanoscale distribution of mitochondrial import receptor Tom20 is adjusted to cellular conditions and exhibits an inner-cellular gradient. *Proc. Natl. Acad. Sci. USA* **108**: 13546–13551.

Arabidopsis Seed Mitochondria Are Bioenergetically Active Immediately upon Imbibition and Specialize via Biogenesis in Preparation for Autotrophic Growth

Gaël Paszkiewicz, José M. Gualberto, Abdelilah Benamar, David Macherel and David C. Logan
Plant Cell 2017;29;109-128; originally published online January 6, 2017;
DOI 10.1105/tpc.16.00700

This information is current as of April 26, 2017

Supplemental Data	http://www.plantcell.org/content/suppl/2017/01/06/tpc.16.00700.DC1.html
References	This article cites 51 articles, 26 of which can be accessed free at: http://www.plantcell.org/content/29/1/109.full.html#ref-list-1
Permissions	https://www.copyright.com/ccc/openurl.do?sid=pd_hw1532298X&issn=1532298X&WT.mc_id=pd_hw1532298X
eTOCs	Sign up for eTOCs at: http://www.plantcell.org/cgi/alerts/ctmain
CiteTrack Alerts	Sign up for CiteTrack Alerts at: http://www.plantcell.org/cgi/alerts/ctmain
Subscription Information	Subscription Information for <i>The Plant Cell</i> and <i>Plant Physiology</i> is available at: http://www.aspb.org/publications/subscriptions.cfm